the new subpopulation that occurred after axonal injury—gradually increased, reaching a maximum at 2 weeks, and then remained unchanged until postoperative week 7 although the immunoreactivity of HSP27 appeared to decrease at 7 weeks. Thus, we consider that axonal injury induced the simultaneous upregulation of the two proteins in small neurons. On the other hand, Gonzalez-Hernandez and Rustioni (1999) used the same model as presented here to show that NOS-immunoreactive neurons were coexpressed with growth-associated phosphoprotein 43 (GAP-43), and this coexpression was also seen in the regenerating axons in the sciatic nerve. They concluded that NO might contribute to the growth and regeneration of injured axons. In our study, NOS-immunoreactive fibers showing regenerating profiles appeared at 2–4 weeks when the NOS-immunoreactive neurons were maximum both in number and immunoreactivity; this might support the conclusion drawn by the previous authors. Thus, we suppose that both proteins examined in our study, NOS and HSP27, might play a neuroprotective role in small DRG neurons. The coexpression of these proteins in small neurons might also indicate that axonal damage causes a more protective neuronal response in small neurons than other larger-sized subpopulations.

The present study also demonstrated that the maximal level of NOS-immunoreactive neurons was maintained until 7 weeks after nerve injury. This finding is consistent with a previous study using sciatic nerve transection models (Fiallos-Estrada *et al.*, 1993), in which the considerable increase in NOS-immunoreactive DRG neurons persisted even until 21 weeks after transection. The lengthy expression of NOS in the small DRG neurons may be explained by the occurrence of the NOS-immunoreactive baskets surrounding NOS negative large neurons since they were formed by axonal sprouts from NOS-immunoreactive small neurons and appeared after depletion of the NOS-immunoreactive regenerating fibers in the sciatic nerve.

It has not been previously described how the NOS-containing pericellular baskets appear in the DRG after peripheral axotomy although a few studies using other neuronal markers reported the occurrence of similar structures. McLachlan *et al.* (1993) first showed that noradrenergic perivascular axons sprout in the DRGs and form basket-like structures around axotomized large DRG neurons. They thought that these unusual connections, along with the sprouting of Aβ axons terminating deep in the dorsal horn into Lamina II (Woolf *et al.*, 1992), contribute to the changes in sensory processing that might lead to neuropathic pain. Further studies demonstrated that the similar pericellular baskets were also formed by axonal sprouts of calcitonin gene-related peptide and substance P-positive small DRG neurons (McLachlan and Hu, 1998) and Isolectin B4-positive small DRG neurons(Li and Zhou, 2001), preferentially around large neurons after peripheral axotomy.

The mechanism for the formation of the pericellular baskets remains obscure. Li and Zhou (2001) assumed that changes in the neurotrophic environment encountered by small and large injured sensory neurons might lead to a rewiring of these neurons in the DRGs and spinal cord. We consider that the formation of NOS-immunoreactive pericellular baskets might be performed by a similar mechanism since trophic factors such as NGF are reportedly involved in the induction of NOS in small neurons (for review see Thippeswamy and Morris, 2002).

As one of the functions of induced NOS after peripheral nerve injury, it has been proposed that NO might play a role in nociceptive transmission in chronic neuropathic pain (Meller *et al.*, 1992; Choi *et al.*, 1996; Cizkova *et al.*, 2002) although Luo *et al.* (1999) cast doubt on this assumption. Retrograde labeling confirmed that both the small neurons sending the NOS-immunoreactive axonal sprout that formed the pericellular basket and the large neurons surrounded by it were axotomized. Thus, our study is first to reveal that peripheral axotomy induces abnormal connections between NOS-immunoreactive small neurons and NOS negative large neurons, suggesting the involvement of NO in rewiring these two classes of primary sensory neurons. However, further studies are needed to clarify whether NO is associated with the development of neuropathic pain.

Acknowledgements

We thank Mr. Takaaki Kanemaru (Morphology Core, Graduate School of Medical Sciences, Kyushu University) and Mr. Yasuhiro Hirakawa for their help in preparing photomicrographs, and Mr. Naoya Inakura for his expert technical assistance.

References

Bredt DS, Snyder SH: Isolation of nitric oxide synthetase, a calmodulin-requiring enzyme. *Proc Natl Acad Sci USA* 87: 682-685 (1990).

Cajal YR: *Degeneration and regeneration of the nervous system* (May RM, ed), Vol. 1. Hafner Publishing Co., NY, 1959 (p. 290-304).

Choi Y, Raja SN, Moore LC, Tobin JR: Neuropathic pain in rats is associated with altered nitric oxide synthase activity in neural tissue. *J Neurol Sci* 138: 14-20 (1996).

Ciocca DR. Oesterreich S. Chamness GC. McGuire WL. Fuqua SA: Biological and clinical implications of heat shock protein 27,000 (Hsp27): a review. *J Natl Cancer Inst* 85: 1558-1570 (1993).

Cizkova D, Lukacova N, Marsala M, Marsala J: Neuropathic pain is associated with alterations of nitric oxide synthase immunoreactivity and catalytic activity in dorsal root ganglia and spinal dorsal horn. *Brain Res Bull* 58: 161-171 (2002).

Costigan M, Mannion RJ, Kendall G, Lewis SE, Campagna JA, Coggeshall RE, Meridith-Middleton J, Tate S, Woolf CJ: Heat shock protein 27: developmental regulation and expression after peripheral nerve injury. *J Neurosci* 18: 5891-5900 (1998).

Estevez AG, Spear N, Manuel SM, Radi R, Hendersin CE, Barbeito L, Beckman JS: Nitric oxide and superoxide contribute to motor neuron apoptosis induced by trophic factor deprivation. *J Neurosci* 18: 923-931 (1998).

Fiallos-Estrada CE, Kummer W, Mayer B, Bravo R, Zimmermann M, Herdegen T: Long-lasting increase of nitric oxide synthase immunoreactivity, NADPH-diaphorase reaction and c-JUN co-expression in rat dorsal root ganglion neurons following sciatic nerve transection. *Neurosci Lett* 150: 169-173 (1993).

Gonzalez-Hernandez T, Rustioni A: Nitric oxide synthase and growth-associated protein are coexpressed in primary sensory neurons after peripheral injury. *J Comp Neurol* 404: 64-74 (1999).

He J, Hirata K, Wang S, Kawabuchi M: Expression of nitric oxide synthase and 27-kD heat shock proteins in motor neurons of ventral root-avulsed rats. *Arch Histol Cytol* 66: 83-93 (2003).

Head MW, Corbin E, Goldman JE: Coordinate and independent regulation of alpha B-crystallin and hsp27 expression in response to physiological stress. *J Cell Physiol* 159: 41-50 (1994).

Hirata K, He J, Hirakawa Y, Liu W, Wang S, Kawabuchi M: HSP27 is markedly induced in Schwann cell columns and the associated regenerating axons. *Glia* 42: 1-11 (2003).

Iadicola C: Bright and dark sides of nitric oxide in ischemic brain injury. *Trends Neurosci* 20: 132-139 (1997).

Imura T, Shimohama S, Sato M, Nishikawa H, Madono K, Akaike A, Kimura J: Differential expression of small heat shock proteins in reactive astrocytes after focal ischemia: possible role of beta-adrenergic receptor. *J Neurosci* 19: 9768-9779 (1999).

Iwaki T, Iwaki A, Tateishi J, Sakaki Y, Goldman JE: Alpha B-crystallin and 27-kd heat shock protein are regulated by stress conditions in the central nervous system and accumulate in Rosenthal fibers. *Amer J Pathol* 143: 487-495 (1993).

Kato H, Liu Y, Kogure K, Kato K: Induction of 27-kDa heat shock protein following cerebral ischemia in a rat model of ischemic tolerance. *Brain Res* 634: 235-244 (1994).

Kato H, Kogure K, Liu XH, Araki T, Kato K, Itoyama Y: Immunohistochemical localization of the low molecular weight stress protein HSP27 following focal cerebral ischemia in the rat. *Brain Res* 679: 1-7 (1995).

Kobayashi S, Koyama J, Yokouchi K, Fukushima N, Oikawa S, Moriizumi T: Functionally essential neuronal population of the facial motor nucleus. *Neurosci Res* 45:357-361 (2003).

Krumenacker JS, Hanafy KA, Murad F: Regulation of nitric oxide and soluble guanylyl cyclase. *Brain Res Bull* 62: 505-515 (2004).

Lewis SE, Mannion RJ, White FA, Coggeshall RE, Beggs S, Costigan M, Martin JL, Dillmann WH, Woolf CJ: A role for HSP27 in sensory neuron survival. *J Neurosci* 19: 8945-8953 (1999).

Li L, Zhou XF: Pericellular Griffonia simplicifolia I isolectin B4-binding ring structures in the dorsal root ganglia following peripheral nerve injury in rats. *J Comp Neurol* 439: 259-274 (2001).

Luo ZD, Chaplan SR, Scott BP, Cizkova D, Calcutt NA, Yaksh TL: Neuronal nitric oxide synthase mRNA upregulation in rat sensory neurons after spinal nerve ligation: lack of a role in allodynia development. *J Neurosci* 19: 9201-9208 (1999).

McLachlan EM, Hu P: Axonal sprouts containing calcionin gene-related peptide and substance P form pericellular baskets around large diameter neurons after sciatic nerve transection in the rat. *Neuroscience* 84: 961-965 (1998).

McLachlan EM, Janig W, Devor M, Mivhaelis M: Peripheral nerve injury triggers noradrenergic sprouting within dorsal root ganglia. *Nature* 363: 543-546 (1993).

Meller ST, Pechmans PS, Gebhart GF, Maves TJ: Nitric oxide mediates the thermal hyperalgesia prodeced in a model of neuropathic pain in the rat. *Neuroscience* 50: 7-10 (1992).

Novikov L, Novikova L, Kellerth JO: Brain-derived neurotrophic factor promotes survival and blocks nitric oxide synthase expression in adult rat spinal motoneurons after ventral root avulsion. *Neurosci Lett* 200: 45-48 (1995).

Plumier JC, Armstrong JN, Landry J, Babity JM, Robertson HA, Currie RW: Expression of the 27,000 mol. wt heat shock protein following kainic acid-induced status epilepticus in the rat. *Neuroscience* 75: 849-856 (1996).

Renkawek K, Bosman GJ, de Jong WW: Expression of small heat-shock protein hsp 27 in reactive gliosis in Alzheimer disease and other types of dementia. *Acta Neuropathol (Berl)* 87: 155-160 (1994).

Shinohara H, Inaguma Y, Goto S, Inagaki T, Kato K: Alpha B crystallin and HSP28 are enhanced in the cerebral cortex of patients with Alzheimer's disease. *J Neurol Sci* 119: 203-208 (1993).

Thippeswamy T, Morris R: The roles of nitric oxide in dorsal root ganglion neurons. *Ann NY Acad Sci* 962: 103-110 (2002).

Thippeswamy T, Jain RK, Mumtaz N, Morris R: Inhibition of neuronal nitric oxide synthase results in neurodegeneration changes in the axotomised dorsal root ganglion neurons: evidence for a neuroprotective role of nitric oxide in vivo. *Neurosci Res* 40: 37-44 (2001).

Verge VM, Xu Z, Xu XJ, Wiesenfeld-Hallin Z, Hokfelt T: Marked increase in nitric oxide synthase mRNA in rat dorsal root ganglia after peripheral axotomy: in situ hybridization and functional studies. *Proc Natl Acad Sci USA* 89: 11617-11621 (1992).

Woolf CJ, Shortland P, Coggeshall RE: Peripheral nerve injury triggers central sprouting of myelinated afferents. *Nature* 355: 75-78 (1992).

Wu W, Li L: Inhibition of nitric oxide synthase reduces motoneuron death due to spinal root avulsion. *Neurosci Lett* 153: 121-124 (1993).

Wu W, Han K, Li L, Schinco FP: Implantation of PNS graft inhibits the induction of neuronal nitric oxide synthase and enhances the survival of spinal motoneurons following root avulsion. *Exp Neurol* 129: 335-339 (1994).

Zhang X, Verge V, Wiesenfeld-Hallin Z, Ju G, Bredt D, Synder SH, Hokfelt T: Nitric oxide synthase-like immunoreactivity in lumbar dorsal root ganglia and spinal cord of rat and monkey and effect of peripheral axotomy. *J Comp Neurol* 22: 563-575 (1993).

DNA vaccination of HSP105 leads to tumor rejection of colorectal cancer and melanoma in mice through activation of both CD4+ T cells and CD8+ T cells

Masafumi Miyazaki,[1,2,6] Tetsuya Nakatsura,[1,6] Kazunori Yokomine,[1] Satoru Senju,[1] Mikio Monji,[1] Seiji Hosaka,[1] Hiroyuki Komori,[1,2] Yoshihiro Yoshitake,[1] Yutaka Motomura,[1,2] Motozumi Minohara,[4] Tatsuko Kubo,[3] Keiichi Ishihara,[5] Takumi Hatayama,[5] Michio Ogawa[2] and Yasuharu Nishimura[1,6]

[1]Department of Immunogenetics, [2]Department of Surgery II, and [3]Department of Molecular Pathology, Graduate School of Medical Sciences, Kumamoto University, 1-1-1 Hongo, Kumamoto 860–8556; [4]Department of Neurology, Neurological Institute, Graduate School of Medical Sciences, Kyushu University, 3-1-1 Maidashi, Higashi-ku, Fukuoka 812-8582; and [5]Department of Biochemistry, Kyoto Pharmaceutical University, 5 Nakauchi-cho, Misasagi, Yamashina-ku, Kyoto 607-8414, Japan

(Received May 25, 2005/Revised July 7, 2005/Accepted July 11, 2005/Online publication August 29, 2005)

We report that HSP105, identified by serological identification of antigens by recombinant expression cloning (SEREX), is overexpressed in a variety of human cancers, including colorectal, pancreatic, thyroid, esophageal, and breast carcinoma, but is not expressed in normal tissues except for the testis. The amino acid sequences and expression patterns of HSP105 are very similar in humans and mice. In this study, we set up a preclinical study to investigate the usefulness of a DNA vaccine producing mouse HSP105 whole protein for cancer immunotherapy *in vivo* using BALB/c and C57BL/6 mice, Colon26, a syngeneic endogenously HSP105-expressing colorectal cancer cell line, and B16.F10, a melanoma cell line. The DNA vaccine was used to stimulate HSP105-specific T-cell responses. Fifty percent of mice immunized with the *HSP105* DNA vaccine completely suppressed the growth of subcutaneous Colon26 or B16.F10 cells accompanied by massive infiltration of both CD4+ T cells and CD8+ T cells into tumors. In cell transfer or depletion experiments we proved that both CD4+ T cells and CD8+ T cells induced by these vaccines play critical roles in the activation of antitumor immunity. Evidence of autoimmune reactions was not present in surviving mice that had rejected tumor cell challenges. We found that HSP105 was highly immunogenic in mice and that the *HSP105* DNA vaccination induced antitumor immunity without causing autoimmunity. Therefore, HSP105 is an ideal tumor antigen that could be useful for immunotherapy or the prevention of various human tumors that overexpress HSP105, including colorectal cancer and melanoma. (*Cancer Sci* 2005; 96: 695–705)

Colorectal cancer (CRC) and melanoma are common and serious malignancies, for which surgery remains the main treatment, although the success of the treatment depends on the stage of the disease. Although adjuvant systemic chemotherapy or chemoradiation can confer a limited but significant survival advantage, novel and more effective therapies are needed. Identification of tumor associated antigens (TAA) expressed by CRC or melanomas remains one of the goals for designing novel immunological treatments for these tumors. Ideal targets for immunotherapy are gene products that are silenced in normal tissues except immune privilege tissue such as testis tissue, and that are overexpressed in cancer cells.

More than 2000 candidate TAA have been identified by using the serological identification of antigens by recombinant expression cloning (SEREX) method. We have also reported TAA identified by using this method.[1–4] We earlier found that HSP105 (often called HSP110), as identified by SEREX was overexpressed specifically in a variety of human cancers, including colorectal, pancreatic, thyroid, esophageal, and breast carcinoma, but was not expressed in normal tissues except for testis tissue.[1,5] We recently found that HSP105 was also overexpressed in melanoma (unpublished data). If HSP105 can induce strong antitumor immunity, it may be a potential candidate as a target antigen for cancer immunotherapy. In the present study, we set up a preclinical study to investigate the usefulness of a *HSP105*-DNA vaccine, using BALB/c and C57BL/6 mice, the syngeneic endogenously HSP105-expressing CRC cell line Colon26, and the melanoma cell line B16.F10. Using these models, we analyzed both the antitumor effects and side-effects, including autoimmunity of the *HSP105* DNA vaccination.

The pioneering studies of Srivastava and colleagues led to the proposal that several HSP, including HSP70, HSP90 and gp96, bind antigenic peptides and deliver these peptides (through receptor-mediated endocytosis of the HSP) into the antigen-processing pathway of the antigen presenting cell (APC) for presentation on major histocompatibility complex (MHC) class I molecules. This HSP-involved pathway has been demonstrated to evoke potent antiviral and antitumor immune responses.[6] However, many researchers have identified MHC class I-presented peptide epitopes derived from HSP. HSP are

M. Miyazaki and T. Nakatsura contributed equally to this work.
[6]To whom correspondence should be addressed. E-mail: mxnishim@gpo.kumamoto-u.ac.jp or tnakatsu@kaiju.medic.kumamoto-u.ac.jp
Abbreviations: C26 (C20), Colon26 clone 20; CRC, colorectal cancer; CTL, cytotoxic T lymphocytes; HE, hematoxylin and eosin; HSP105, heat shock protein 105; APC, antigen presenting cell; mAb, monoclonal antibody; MHC, major histocompatibility complex; SEREX, serological identification of antigens by recombinant expression cloning; TAA, tumor associated antigens.

 doi: 10.1111/j.1349-7006.2005.00093.x

rich sources of MHC-bound peptides, and the expression of these peptides increases as a result of cellular stresses.[7]

Recently, Subjeck and colleagues tested a vaccine using the chaperoning properties of HSP110 as Srivastava and colleagues had done before them.[8,9] They reported that HSP110 overexpression increases the immunogenicity of murine CT26 colon tumors.[10] *HSP110* cloned from CHO cells[11] and *HSP105* cloned from mice[12] and humans[13] are homologs. We show here that this HSP105 is highly immunogenic for stimulating tumor immunity against mouse CRC and melanoma. Furthermore, both $CD4^+$ T cells and $CD8^+$ T cells induced by the *HSP105* DNA vaccination play critical roles in the activation of antitumor immunity. These findings indicate that HSP105 itself could be considered a valuable TAA for the immune-based therapy of various tumors overexpressing HSP105, including CRC and melanoma.

Materials and Methods

Cell lines and mice

A subline of the BALB/c-derived CRC cell line Colon26, C26 (C20),[14] was provided by Dr Kyoichi Shimomura (Fujisawa Pharmaceutical Co., Japan). B16.F10 was kindly provided by the Cell Resource Center for Biomedical Research, Institute of Development, Aging, and Cancer, Tohoku University (Sendai, Japan). These cell lines were maintained *in vitro* in RPMI-1640 medium supplemented with 10% fetal calf serum at 37°C in a 5% CO_2 atmosphere. Female 7-week-old BALB/c mice ($H\text{-}2^d$) and C57BL/6 mice ($H\text{-}2^b$), purchased from Charles River Japan (Yokohama, Japan), were kept in the Center for Animal Resources and Development (CARD) of Kumamoto University, and handled in accordance with the animal care policy of Kumamoto University.

Histological and immunohistochemical analysis

Immunohistochemical detections of HSP105, CD8 and CD4 were carried out as described elsewhere.[1,5,15–18] The primary antibody used in this study, rabbit polyclonal antihuman HSP105 was purchased from Santa Cruz (Santa Cruz, CA, USA). Hematoxylin and eosin (HE) staining and standard methods were used for histological analysis. We purchased Human Normal Organs and Cancer Multi Tissue Slide, BC4, from SuperBioChips Laboratories (Seoul, Korea) for immunohistochemical analysis.

Construction of a mouse *HSP105* expression plasmid DNA

Plasmid pcDNA105, which expresses mouse *HSP105* whole protein was generated as described elsewhere.[12] To construct this plasmid, the mouse *HSP105* full-length cDNA derived from the pB105-1 plasmid was subcloned into *Eco*RV–*Xba*I sites of the mammalian expression vector pcDNA3 (Invitrogen, Osaka, Japan). The pCAGGS expression vector was kindly provided by Dr Junichi Miyazaki (Osaka University, Japan) and this vector induces strong gene expression when injected into muscle.[19] We constructed a pCAGGS-*HSP105* plasmid by inserting mouse *HSP105* cDNA into the *Eco*RI site of the pCAGGS expression vector, which carries the CAG (cytomegalovirus immediate-early enhancer/chicken β-actin hybrid) promoter, and prepared the plasmid using a Qiagen EndoFree plasmid Mega kit (Qiagen GmbH, Hilden, Germany). We used the empty pCAGGS plasmid as a control.

DNA vaccination

We immunized mice twice by intramuscular injection into the anterior tibialis muscle. Booster immunization was carried out at 7 days after the primer immunization. The groups of mice were given the following vaccines: (i) saline group: given with 100 μL saline; (ii) control vector group: given 50 μg pCAGGS plasmids lacking inserts and diluted in 100 μL saline; (iii) *HSP105* DNA vaccine group: given 50 μg of pCAGGS-*HSP105* plasmid diluted in 100 μL saline.

In vivo tumor challenge

Subcutaneous tumors were established by the injection of 3×10^4 C26 (C20) cells or 1×10^4 B16.F10 cells suspended in 100 μL Hanks' Balanced Salt Solution (Gibco, Grand Island, NY, USA) medium into the right flank of BALB/c or C57BL/6 mice 7 days after the last vaccination. Tumor incidence and volume were assessed twice weekly using calipers until the mice died. Tumor area was calculated as a product of width and length. The results are presented as mean area of tumor ± SE; however, individual tumor area is presented for some experiments.

In vivo depletion of $CD4^+$ T cells and $CD8^+$ T cells

Each mouse was given a total of six intraperitoneal transfers (days −18, −15, −11, −8, −4, −1) of ascites (0.1 mL per mouse per transfer) from hybridoma-bearing nude mice. The mAbs used were rat antimouse CD4 (clone GK1.5) and rat antimouse CD8 (clone 2.43). Normal rat IgG (Sigma, St. Louis, MO, USA; 200 μg per mouse per transfer) was used as a control. The depletion of T cell subsets by treatment with mAbs was confirmed by flow cytometric analysis of spleen cells, which showed a > 90% specific depletion.

Cell transfer *in vivo*

We purified $CD8^+$ T cells, $CD4^+$ T cells, and natural killer (NK) cells from spleen cells using the magnetic cell sorting system with antimouse CD8α (Ly-2) mAb, antimouse CD4 (L3T4) mAb, antimouse NK (DX5) mAb, and these $CD8^+$ T cells, $CD4^+$ T cells, and NK cells were used for adoptive transfer into BALB/c mice. To investigate tumor growth in a homeostatic lymphocyte proliferation model, we intravenously injected 1.5×10^7 whole spleen cells or 3×10^6 $CD8^+$ T cells, $CD4^+$ T cells, NK cells, or $CD8^-$ $CD4^-$ NK^- cells 3 days after sublethal irradiation (5 Gy). Subsequently, we subcutaneously inoculated BALB/c mice with C26 cells (3×10^4) 3 days after irradiated mice inoculated with cells.

Statistical analysis

We analyzed all data using the StatView statistical program for Macintosh (SAS, Cary, NC, USA) and evaluated statistical significance using the unpaired *t*-test. The overall survival rate was calculated using the Kaplan–Meier method, and statistical significance was evaluated using Wilcoxon's test.

Results

Similar tissue and cancer-specific expression of HSP105 in mice and humans

We have previously reported that HSP105 is overexpressed in a variety of human cancers, including colorectal, pancreatic, esophageal, thyroid, and breast cancer, whereas HSP105 is

 doi: 10.1111/j.1349-7006.2005.00093.x

expressed at low levels in many normal tissues, except for testis tissue.[1,5] In the present study, we carried out an immunohistochemical analysis of HSP105 using various human and mouse tissues (Fig. 1). Human HSP105 is overexpressed in almost all CRC cells, melanoma cells (unpublished data), and normal testis tissue, but there is no expression or only a low-level expression of HSP105 in normal liver, brain, spleen, lung, and kidney tissue (Fig. 1a). Mouse HSP105 is also overexpressed in liver metastasis of the murine colorectal adenocarcinoma cell line C26 (C20), lung metastasis of the murine melanoma cell line B16.F10 and normal testis tissue, but there is no expression or only low-level expression in normal liver, cerebrum, cerebellum, spleen, lung, and kidney tissue (Fig. 1b). Another group reported that HSP105/110 is expressed in neurons in the cerebrum and Purkinje cells in the cerebellum,[20] we found the same pattern in the present study, but the level of expression in the neurons and Purkinje cells was much weaker than that in CRC and testis tissue (Fig. 1a,b). As a result, the expression levels of HSP105 protein in human colorectal, pancreatic, esophageal, thyroid, and breast cancers, melanoma, C26 tumors, and B16.F10 tumors were evidently much higher than those in all normal adult tissues, including brain, but not testis in both humans and mice. Because the expression pattern of HSP105 is very similar in humans and mice, we are able to analyze both the antitumor effects and side-effects (including autoimmunity) of HSP105 vaccination using this mouse model of CRC and melanoma.

HSP105 DNA induced rejection of C26 and B16.F10 tumor challenge in mice

We investigated the effects of *HSP105* DNA vaccination using a subcutaneously injected C26 (Fig. 2a–d) and B16.F10 (Fig. 2e–h) tumor model. Mice were divided into three groups: mice inoculated with (i) saline; (ii) pCAGGS, and (iii) pCAGGS-*HSP105*. No mice died during the vaccination period.

Subcutaneous inoculation of C26 cells (3×10^4) into the right flank was given 7 days after the last vaccination (Fig. 2a–d). In groups (i) and (ii), subcutaneous tumors appeared in some mice 10 days after inoculation. Measurement of tumor size was continued until 24 days after inoculation with the tumor cells, when one mouse died. The mean tumor size on day 24 in group (iii) mice (26.4 ± 10.8 mm^2) was significantly smaller than that in the other two groups (105.0 ± 15.7, and 86.0 ± 8.3 mm^2, respectively; $P < 0.05$; Fig. 2a). Six of the 10 mice (60%) in group (iii) did not have subcutaneous tumors on day 24 (Fig. 2b). All mice in groups (i) and (ii) had subcutaneous tumors within 13 days, and died within 41 days of inoculation with the tumor cells (Fig. 2c,d). Five of the 10 mice (50%) in group (iii) completely rejected the 3×10^4 C26 cells during the 108 days after the inoculation (Fig. 2c,d). A statistically significant difference in survival time was found between group (iii) and groups (i) and (ii) ($P < 0.05$).

Subcutaneous inoculation of B16.F10 cells (1×10^4) into the right flank was carried out 7 days after the last vaccination (Fig. 2e–h). Measurement of tumor size was continued until 30 days after inoculation with the tumor cells, when one mouse died. Mean tumor size on day 30 in group (iii) mice (103.9 ± 49.8 mm^2) was significantly smaller than that in the other two groups (272.1 ± 69.7, and 361.6 ± 50.3 mm^2, respectively; $P < 0.05$; Fig. 2e). Six of eight mice (75%) in group (iii) did not have subcutaneous tumors on day 30 (Fig. 2f). All mice in groups (i) and (ii) had subcutaneous tumors within 41 days, and died within 65 days of inoculation with the tumor cells (Fig. 2g,h). Four of eight mice (50%) in group (iii) completely rejected the 1×10^4 B16.F10 cells during the 100 days after the inoculation (Fig. 2g,h). A statistically significant difference in survival time was found between group (iii) and groups (i) and (ii) ($P < 0.05$). Therefore, the *HSP105* DNA vaccine has the potential to prevent the growth of tumors expressing HSP105.

We also subcutaneously inoculated five surviving group (iii) mice that completely rejected the first challenges with C26 cells with further (3×10^4) C26 cells. These mice also rejected the second challenge with C26 cells, even at 108 days after the first challenge (data not shown). These results demonstrate that the effects of vaccination in group (iii) continued for a long time, and that the vaccination prevented the recurrence of HSP105-expressing tumors.

Expression of HSP105 protein and infiltration of CD4$^+$ T cells and CD8$^+$ T cells in the injection sites

To observe HSP105 expression and infiltrating cells in muscles injected with the *HSP105* DNA vaccine, we carried out intramuscular immunizations with pCAGGS DNA into the right anterior tibialis muscle, and with pCAGGS-*HSP105* DNA into the left anterior tibialis muscle of four mice. After 48 h, we killed the mice and evaluated the muscles by histological and immunohistochemical analysis (Fig. 3). In HE-stained sections, there were some transverse sections of injection sites that included many cells in both the pCAGGS- and pCAGGS-*HSP105*-immunized muscles. But only in the transverse sections of the injection sites in pCAGGS-*HSP105*-immunized muscles could we observe many cells expressing HSP105 at a high level, and also a considerable number of both CD4$^+$ T cells and CD8$^+$ T cells. Although we did not immunohistochemically stain the dendritic cells in these traverse sections, we did find some dendritic cell-like large cells.

Infiltration of CD4$^+$ T cells and CD8$^+$ T cells into the C26 tumor after vaccination

To observe the antitumor effects of *HSP105 DNA*-vaccination, we evaluated the tumor using immunohistochemical staining of CD8 and CD4. Figure 4a shows the tumor inoculation sites from two *HSP105* DNA-immunized mice, a saline-inoculated mouse, and a pCAGGS-immunized mouse that did not reject the tumor challenge. There were few lymphocytes in the tumors removed from both the saline-inoculated mouse and the pCAGGS immunized mouse, but there were many CD4$^+$ T cells and considerable numbers of CD8$^+$ T cells making contact with the tumor cells and surrounding the tumors removed from the two *HSP105* DNA-immunized mice. These layers of CD4$^+$ T cells surrounding the tumor were thick in the case of *HSP105 DNA* vaccinated mice. Furthermore, there were a considerable number of CD8$^+$ T cells and CD4$^+$ T cells that had infiltrated into the tumor (Fig. 4a).

Vaccination with *HSP105* DNA did not induce damage of normal tissues

HSP105 expression in normal adult mice is limited to several tissues, and HSP105 expression levels in these tissues are

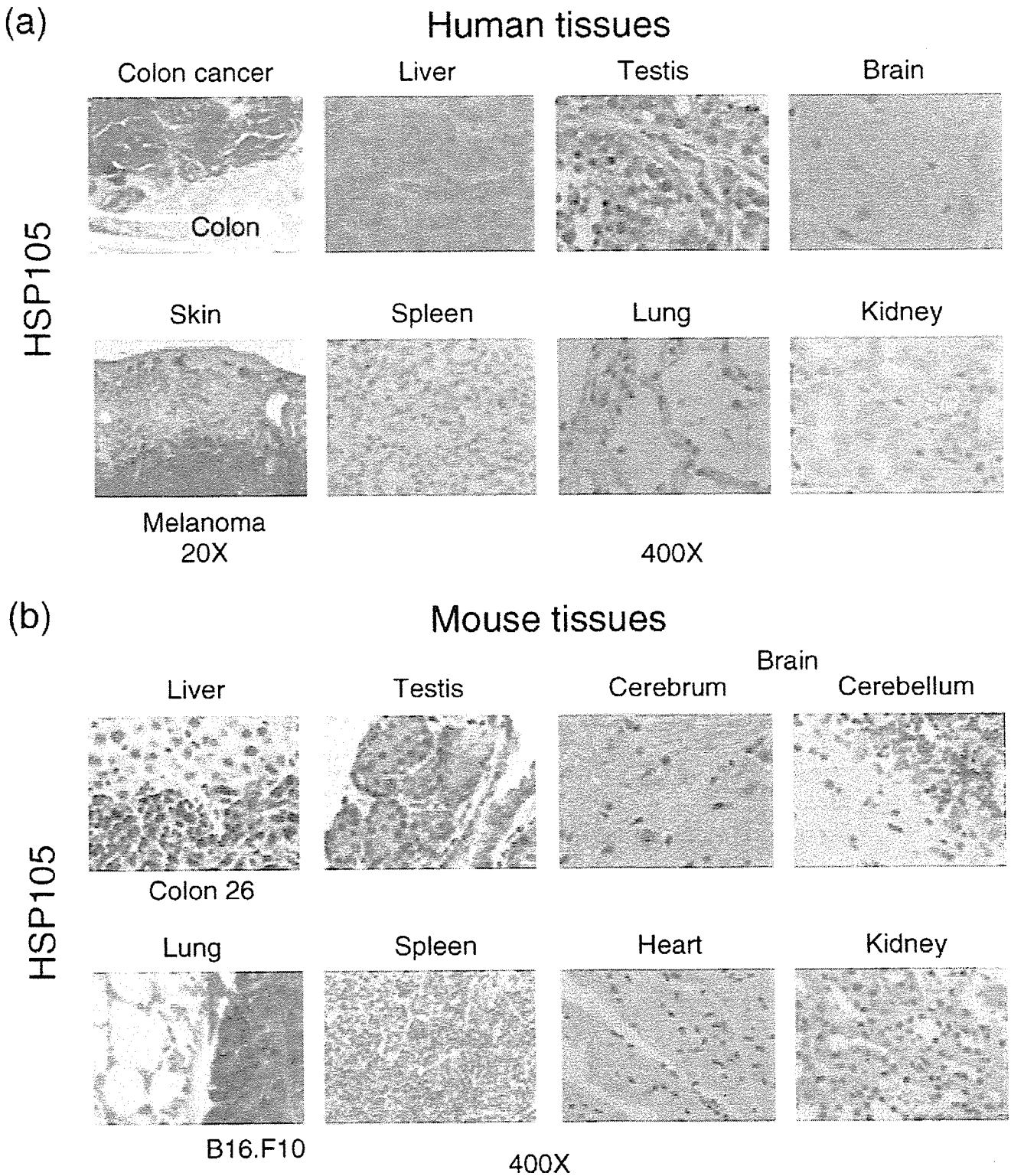

Fig. 1. Expression of the HSP105 protein, a candidate for immunotherapy for CRC and melanoma, in human and mouse tissues and cells. Expression of HSP105 protein detected by immunohistochemical analysis in various (a) human and (b) mouse tissues. Objective magnification was 400× or 20×.

 doi: 10.1111/j.1349-7006.2005.00093.x

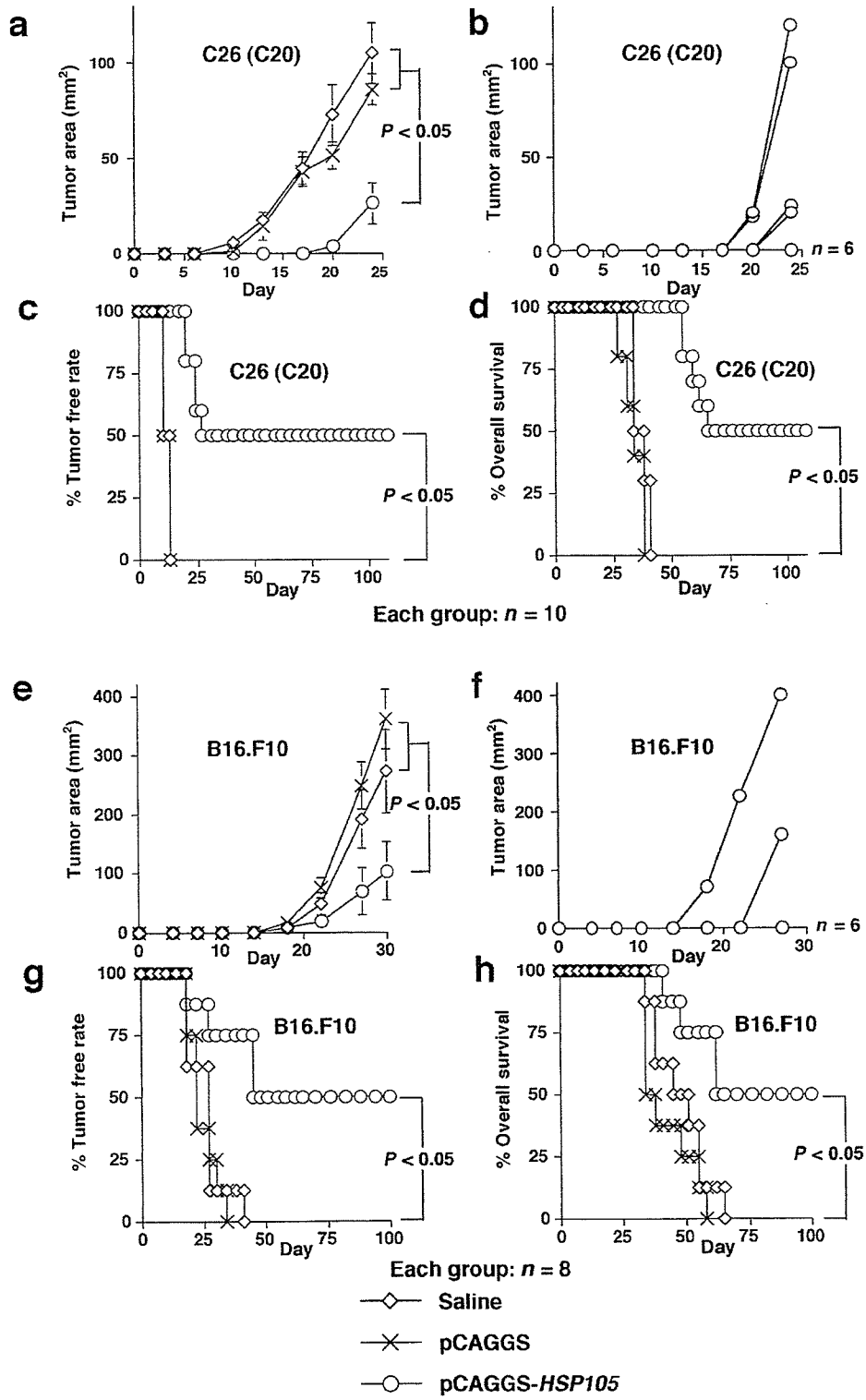

Fig. 2. Vaccination with *HSP105* DNA suppressed the growth of (a–d) C26 and (e–h) B16.F10 tumors in mice. Each group consisted of 10 (a–d) or eight (e–h) mice. (a,b,e,f) Suppression of the growth of HSP105-expressing C26 (a,b) or B16.F10 (e,f) tumors inoculated subcutaneously into mice vaccinated with *HSP105* DNA. The tumor area was calculated as the product of width and length. The result is presented as mean area of tumor ± SE, and we evaluated statistical significance using the unpaired *t*-test (a,e). Growth curves of 10 and eight individual tumors in the mouse group treated with pCAGGS-*HSP105* are presented in (b) and (f), respectively. (c,d,g,h) Percentage tumor free rate (c,g) and percentage overall survival (d,h) were calculated using the Kaplan–Meier method, and the statistical significance of differences between groups was evaluated using Wilcoxon's test.

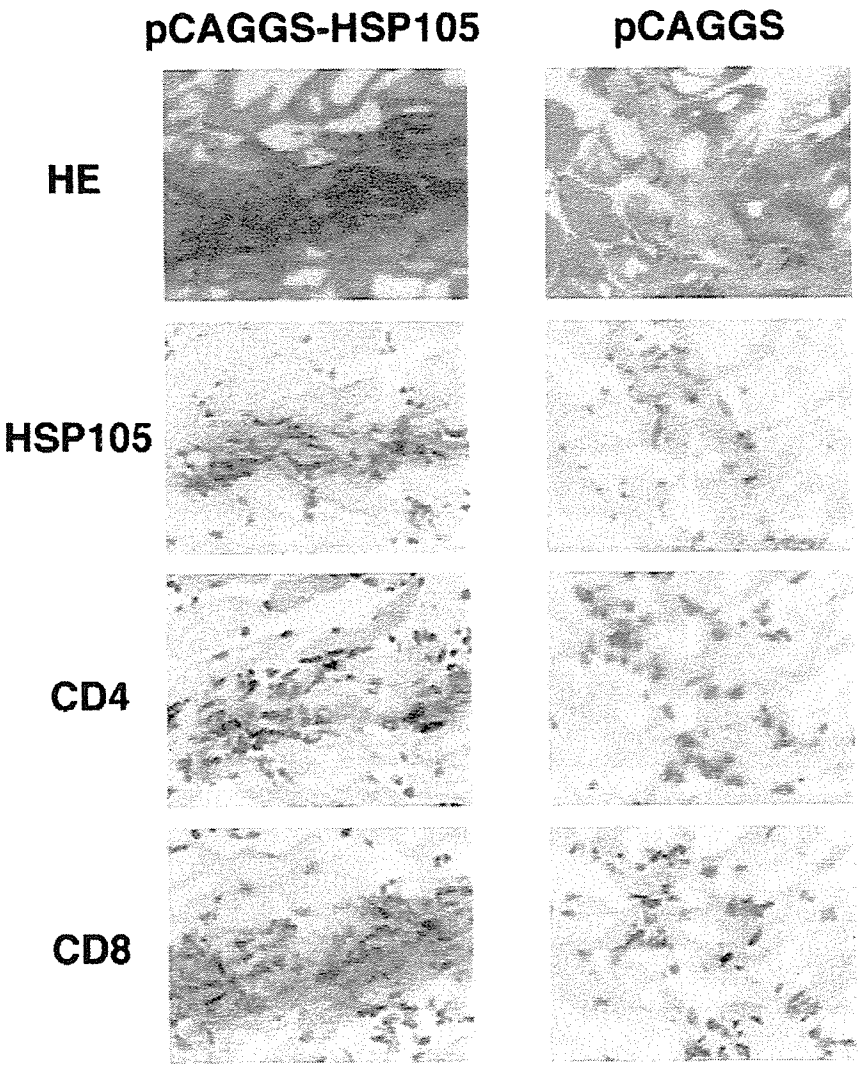

Fig. 3. Expression of HSP105 protein and infiltration of $CD4^+$ T cells and $CD8^+$ T cells in the *HSP105* DNA vaccine-injected sites. To observe HSP105 expression and infiltrating cells in muscles injected with the *HSP105* DNA vaccine, we carried out intramuscular immunizations with pCAGGS-DNA into the right anterior tibialis muscle, and with pCAGGS-*HSP105* DNA into the left anterior tibialis muscle in four mice. After 48 h, we killed the mice and studied their muscle tissue by using HE staining and histological analysis, and immunohistochemical analysis of HSP105, CD4, and CD8. Representative results are shown. Objective magnification was 400×.

lower than those in C26 (C20) tumor cells, which suggests a low risk of damage to normal tissue as a result of immune responses to the HSP105 antigen. To evaluate the risk of autoaggression by immunization against self-HSP105, the tissues of mice immunized with *HSP105* DNA were histologically examined. All mice were apparently healthy, and without abnormalities, suggesting autoimmunity for, for example, dermatitis, arthritis, or neurological disorders. The brain, liver, lung, heart, kidney, and spleen tissues of *HSP105*-immunized mice were critically scrutinized and compared with those of normal mice. These tissues had normal structure and cellularity for each of the two groups examined, and pathological changes caused by immune response, such as infiltrations of $CD8^+$ or $CD4^+$ T cells, or tissue destruction and repair, were not present (Fig. 4b). Although $CD4^+$ T cells and $CD8^+$ T cells infiltrated into the C26 tumor (Fig. 4a), infiltration of $CD4^+$ T cells or $CD8^+$ T cells was not observed in any of the normal adult tissues examined (Fig. 4b). These results indicate that T cells stimulated with the *HSP105* DNA vaccine do not recognize normal cells that express HSP105 at physiological levels.

Anti-C26 tumor adoptive immunity elicited by injection with $CD4^+$ T cells or $CD8^+$ T cells from *HSP105* DNA-vaccinated mice

Antitumor responses could be augmented by homeostatic T cell proliferation in the periphery, involving the expansion of T cells recognizing MHC/tumor antigenic peptide ligands.[21–23] To ascertain that the tumor rejections induced by *HSP105* DNA vaccination were mediated through the activation of $CD8^+$ T cells or $CD4^+$ T cells, in a homeostatic lymphocyte proliferation model, we subcutaneously inoculated BALB/c mice with C26 cells (3×10^4) 6 days after sublethal irradiation (5 Gy). We intravenously injected 1.5×10^7 whole spleen cells or 3×10^6 $CD8^+$ T cells, $CD4^+$ T cells, NK cells, or $CD8^-$ $CD4^-$ NK^- cells derived from each untreated or *HSP105* DNA-vaccinated mouse on day 3 before the tumor inoculation (Fig. 5a). Measurements of tumor size were continued for 22 days after inoculation with the tumor cells (Fig. 5b). Each group consisted of four mice. Inoculation with whole spleen cells or $CD8^+$ T cells, $CD4^+$ T cells, NK cells, or $CD8^-$ $CD4^-$ NK^- cells derived from untreated mice, and with NK cells, or $CD8^-$ $CD4^-$ NK^- cells derived from *HSP105* DNA-vaccinated

 doi: 10.1111/j.1349-7006.2005.00093.x

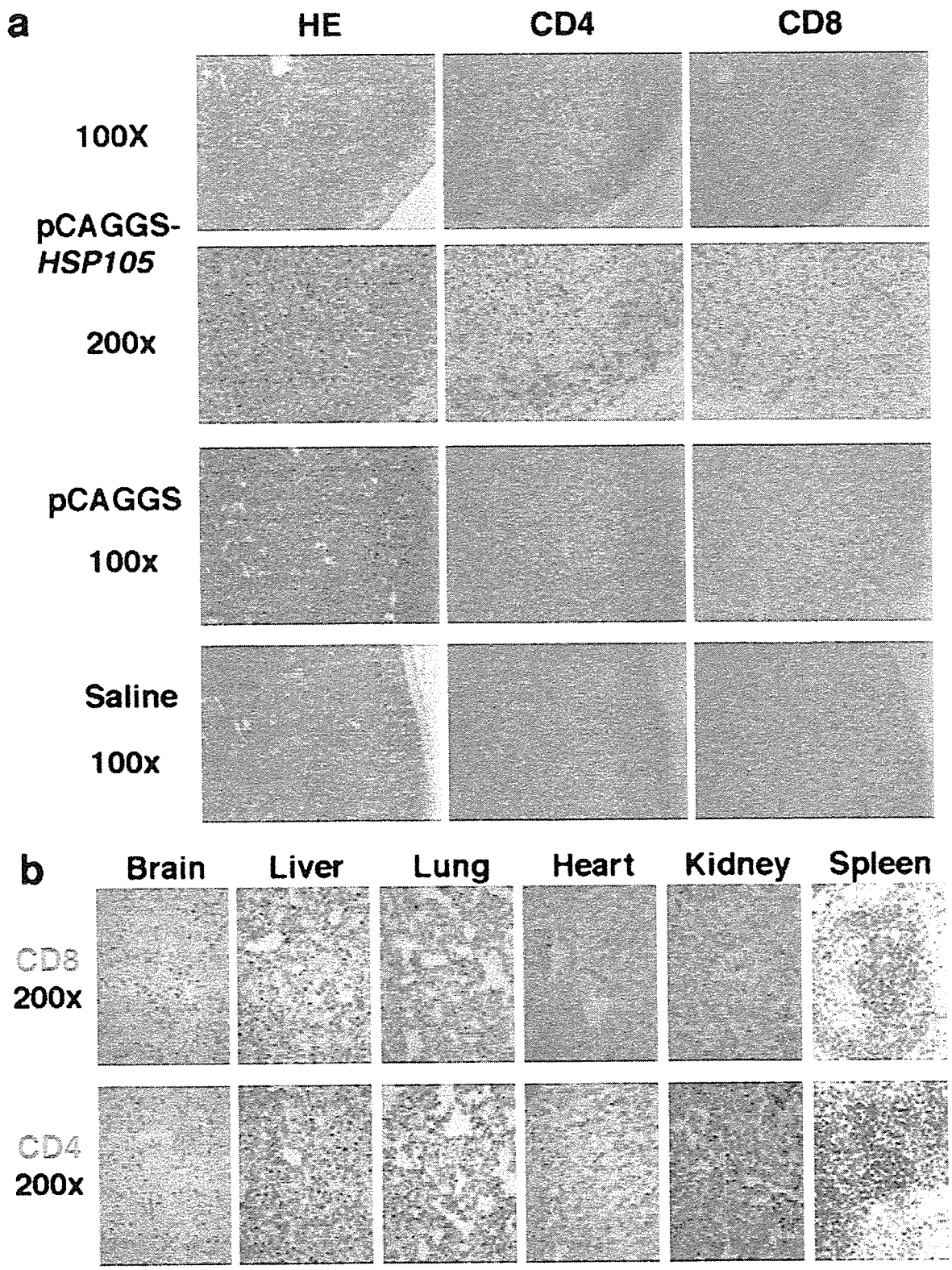

Fig. 4. Vaccination with *HSP105* DNA induced infiltration of both $CD4^+$ T cells and $CD8^+$ T cells into C26 tumors, but not into normal tissues. (a) Subcutaneous C26 tumors removed from two *HSP105* DNA-immunized mice, a saline-inoculated mouse, and a pCAGGS-immunized mouse that did not reject the tumor challenges were analyzed using immunohistochemical staining with anti-CD4 mAb and anti-CD8 mAb. (b) Normal tissues of mice vaccinated with *HSP105* DNA were histologically and immunohistochemically examined. Objective magnification was 200x. The spleen was used as a positive control for staining of both CD4 and CD8.

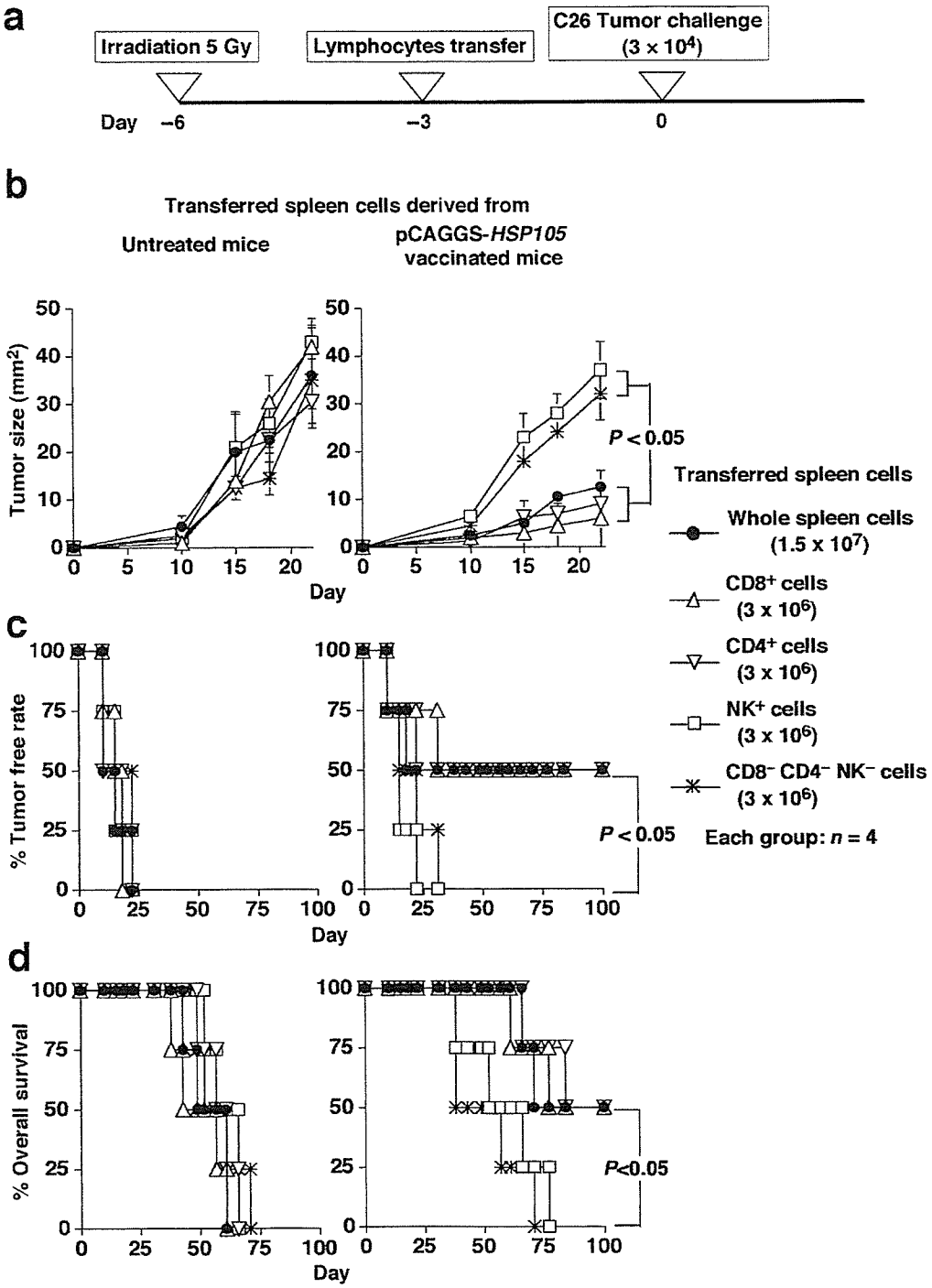

Fig. 5. Injection of either CD4⁺ T cells or CD8⁺ T cells sensitized with *HSP105* DNA vaccine into sublethally irradiated mice elicited effective antitumor adoptive immunity. (a) Experimental protocol; each group consisted of four mice. (b) Suppression of the growth of HSP105-expressing C26 tumors inoculated subcutaneously into mice transferred with each group of spleen cells. Tumor area was calculated as the product of width and length. The result is presented as the mean area of tumor ± SE, and we evaluated the statistical significance using the unpaired *t*-test. (c,d) Percentage tumor free rate (c) and percentage overall survival (d) were calculated using the Kaplan–Meier method, and the statistical significance of differences in survival time between groups was evaluated using Wilcoxon's test.

mice did not cause the mice to reject challenges with C26 cells (3×10^4). Conversely, two of the four mice (50%) that were treated with whole spleen cells, CD8⁺ T cells, or CD4⁺ T cells derived from *HSP105* DNA-vaccinated mice completely rejected challenges with C26 cells (3×10^4; Fig. 5b–d). Thus, sublethally irradiated lymphopenic mice transfused with CD4⁺ T cells or CD8⁺ T cells derived from *HSP105* DNA-vaccinated mice displayed tumor growth inhibition. These results suggest that both CD4⁺ and CD8⁺ T cells play critical roles in antitumor immunity induced by immunization with

 doi: 10.1111/j.1349-7006.2005.00093.x

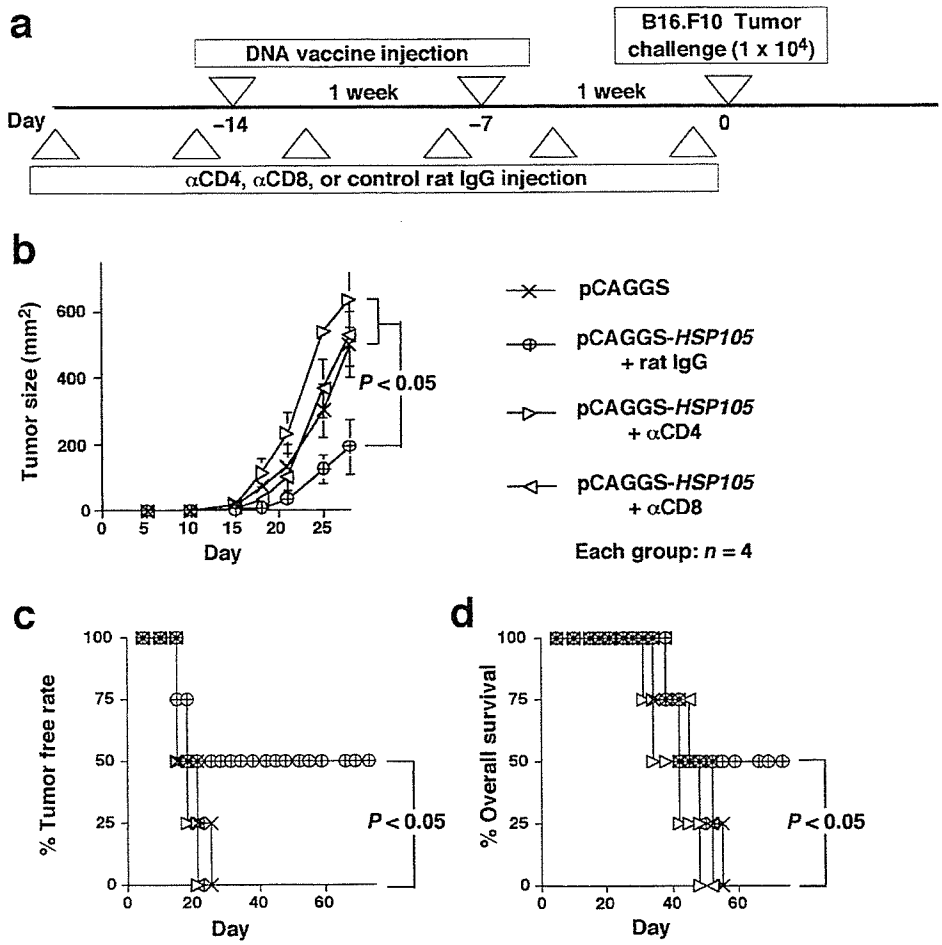

Fig. 6. Involvement of both CD4⁺ T cells and CD8⁺ T cells in protection against B16.F10 induced by vaccination with *HSP105* DNA. (a) Experimental protocol for *in vivo* depletion of CD4⁺ T cells and CD8⁺ T cells. Each group consisted of four mice. (b) Suppression of the growth of HSP105-expressing B16.F10 tumors inoculated subcutaneously into mice vaccinated with *HSP105* DNA. Tumor area was calculated as the product of width and length. Data are presented as mean area of tumor ± SE, and we evaluated the statistical significance using the unpaired *t*-test. (c,d) Percentage tumor free rate (c) and percentage overall survival (d) were calculated using the Kaplan–Meier method, and the statistical significance of differences in survival time between groups was evaluated using Wilcoxon's test.

the *HSP105* DNA-vaccine. The mice shown in Figure 5 were killed more than 100 days after lymphocyte transfer, respectively. All mice were apparently healthy and without abnormalities, suggesting autoimmunity for, for example, dermatitis, arthritis, or neurological disorders. The brain, liver, lung, heart, kidney, and spleen tissues of *HSP105* DNA-immunized mice were critically scrutinized and compared with those of normal mice. These tissues had normal structures and cellularity for each of the two groups examined, and pathological changes caused by immune response, such as CD8⁺ or CD4⁺ T lymphocyte infiltration or tissue destruction and repair, were not present, as shown in Figure 4b. These results indicate that T cells stimulated with HSP105 do not recognize normal cells that express HSP105 at physiological levels.

Involvement of both CD4⁺ T cells and CD8⁺ T cells in protection against B16.F10 induced by *HSP105* DNA-vaccination

To determine the role of CD4⁺ T cells and CD8⁺ T cells in the protection against B16.F10 tumor cells induced by *HSP105* DNA-vaccination, we depleted mice of CD4⁺ T cells or CD8⁺ T cells by treatment with anti-CD4 or anti-CD8 mAb *in vivo*. More than 90% of CD4⁺ T cells or CD8⁺ T cells were depleted (data not shown). During this procedure, mice were immunized with DNA vaccine and challenged with B16.F10 cells (Fig. 6a). Depletion of either CD4⁺ T cells or CD8⁺ T cells almost totally abrogated the protective immunity induced by immunization with *HSP105* DNA vaccine (Fig. 6b–d). These results suggest that both CD4⁺ T cells and CD8⁺ T cells play critical roles in antitumor immunity induced by immunization with *HSP105* DNA vaccine.

Discussion

Advances in molecular biology and tumor immunology have paved the way for identification of a large number of genes encoding TAA and antigenic peptides recognized by tumor-reactive CTL, hence peptide-based cancer immunotherapy has been the focus of much research.[24–26] However, current clinical trials for peptide-based immunotherapy have rarely resulted in tumor regression.[27] The immunogenicity of these

tumor antigenic peptides or the vaccination strategy may be sufficient to induce CTL responses but not to elicit $CD4^+$ T cells.

DNA-based immunization is potentially a powerful method for immunizing against microbial, viral, and tumor antigens through both humoral and cell-mediated immune responses.[28] The generation of T-cell immunity involves local target cell transfection and protein antigen production, which is taken up by host APC, leading to cross-presentation in draining lymph nodes; in addition, direct DNA transfection into APC in peripheral tissue has also been demonstrated.[29] Compared with orthodox vaccines consisting of tumor proteins or viral components, DNA vaccination stimulates host immunity against transgene-encoding proteins without the processes related to protein purification. In the present study, a DNA vaccine was used to activate HSP105-specific tumor immunity.

Although the SEREX method facilitated the identification of tumor antigens that could be recognized by antibodies and $CD4^+$ Th cells, few of their T cell epitopes have been determined.[2,30] We previously reported that HSP105, identified by SEREX of pancreatic adenocarcinoma, was overexpressed specifically in a variety of human cancers, including pancreatic and colon adenocarcinoma.[1,5] Other investigators identified HSP105 by SEREX using other cDNA libraries derived from tissues including colorectal cancer, melanoma, and normal testis. HSP105 are complexes associated with HSP70/HSC70,[31,32] which negatively regulate HSP70/HSC70 chaperone activity.[33] In addition, HSP105 protects neuronal cells against the apoptosis induced by various stresses.[34] HSP105 consists of HSP105α and HSP105β. HSP105α is a constitutively expressed 105-kDa HSP that is induced by a variety of stresses, whereas HSP105β is a 90-kDa HSP that is specifically induced by heat shock at 42°C. HSP105β is a truncated form of HSP105α.[12] We used in this study the mouse HSP105α DNA and protein. Recently, Subjeck and colleagues reported that recombinant HSP110 and cancer antigens such as Her2/*neu* or gp100 complexes are powerful cancer vaccines.[8,9,35] Their HSP110[11] and our HSP105α are in fact the same protein.

Although they noted that HSP110 did not have immunogenic properties, we emphasize in this study that HSP105 does have a strong immunogenic action. Although we did not identify the HSP105-derived epitope peptides of $CD8^+$ T-cells or $CD4^+$ T-cells in this study, we did prove that HSP105 itself could induce both $CD4^+$ T-cells and $CD8^+$ T-cells to become reactive to tumor cells expressing HSP105. As shown in Figure 5, in a homeostatic lymphocyte proliferation model, we demonstrated that adoptive transfer of either $CD4^+$ T cells or $CD8^+$ T cells alone into sublethally irradiated mice was sufficient to reject C26 cells that do not express MHC class II molecules. To ascertain whether this is also true for B16.F10 that express both MHC class I and II molecules in the presence of interferon (IFN)-γ, further investigation is needed. As shown in Figure 6, we demonstrated that both $CD4^+$ T cells and $CD8^+$ T cells were required for rejection of B16.F10 in the induction phase. In terms of the mechanism for the rejection of C26 tumors, we have other data relating to vaccination with HSP105 protein-pulsed BM-DC instead of *HSP105* DNA vaccination. In those experiments, we also demonstrated that both $CD4^+$ T cells and $CD8^+$ T cells were required for rejection of not only B16.F10 but also C26 in the induction phase by depleting $CD4^+$ T cells and $CD8^+$ T cells using the *in vivo* administration of antibodies (unpublished data). Therefore, both HSP105-specific $CD4^+$ T cells and $CD8^+$ T cells seem to be important for the rejection of HSP105-expressing tumors in the induction phase, and either $CD4^+$ T cells or $CD8^+$ T cells can independently exert anti-C26 tumor effects in the effector phase in a homeostatic lymphocyte proliferation model.

It has been reported that antigen-specific $CD4^+$ T-cell help is required to activate memory $CD8^+$ T cells to fully functional effector killer cells.[36] The peptides derived from exogenous antigens acquired by endocytosis are typically presented on MHC class II molecules on the surface of APC, and activate $CD4^+$ T cells. We observed in this study that $CD4^+$ T cells specific to HSP105, in fact, have an important role in tumor rejection, even when tumors do not express MHC class II molecules, such as the C26 tumors used in this study. It was recently reported that tumor-specific $CD4^+$ T cells may have a pivotal role in preventing early tumorigenesis by secreting IFN-γ and stimulating the classical macrophage-activation pathway. This results in the inhibition of tumor cell growth, even when tumor cells themselves do not express MHC class II molecules.[37] To better understand the mechanism of C26 tumor rejection by HSP105-specific $CD4^+$ T cells, further studies are needed. Furthermore, peptides derived from exogenous self-antigen, HSP105, acquired by endocytosis are possibly presented by MHC class I molecules on the surface of APC by cross-presentation to activate $CD8^+$ T cells.

Because HSP are present in all organisms, low levels of human HSP-derived peptides serve as harbingers of autoimmune responses after CTL have been primed to respond to bacterial HSP-derived peptides.[38] However, because many cancers overexpress HSP, CTL-based vaccines that elicit an anti-HSP response might be effective against many different tumors.[39] Indeed, in this study, HSP105 itself evoked T-cell-mediated tumor rejection without autoimmune reactions. In the present paper, all results shown in the figures were obtained using female mice, but we have carried out the same experiment using male mice. *HSP105* DNA vaccination did not induce T-cell infiltration or damage in testis tissue (in which HSP105 is highly expressed). Furthermore, *HSP105* DNA vaccination was also able to induce antitumor immunity in male mice (data not shown), indicating that male mice did not acquire immunological tolerance to HSP105 expressed in testis tissue.

To substantiate the specificity for HSP105, we searched for mouse cancer cell lines derived from BALB/c mice and C57BL/6 mice that do not express HSP105. However, all cancer cell lines we examined strongly expressed HSP105. BALB/3T3 fibroblasts expressed HSP105 relatively weakly, but these cells unfortunately did not form tumors in mice. Further investigations are needed to clarify whether *HSP105* DNA vaccination affects the growth of some tumors that do not express HSP105.

We showed in this study that *HSP105* DNA vaccination can prime T cells to be reactive to tumor cells expressing HSP105 *in vivo*, and that growth of C26 and B16.F10 cells expressing HSP105 was prevented without inducing autoimmune destruction in murine subcutaneous CRC and melanoma models. We believe that *HSP105* DNA vaccination is a novel strategy for the prevention of CRC and melanoma in patients treated surgically who are at high risk of recurrence

 doi: 10.1111/j.1349-7006.2005.00093.x

of CRC or melanoma. Whether or not HSP105 is an ideal target for immunotherapy in human cancers will continue to be investigated in our laboratory.

Acknowledgments

We thank Drs Hidetake Matsuyoshi, Shinya Hirata, Yoshiaki Ikuta, and Daiki Fukuma (Department of Immunogenetics, Graduate School of Medical Sciences, Kumamoto University) for technical assistance, Dr Junichi Miyazaki, Osaka University, for providing the pCAGGS vector, and Dr Kyoichi Shimomura (Fujisawa Pharmaceutical Co.), for providing the cell line. This work was supported in part by Grants-in-Aid (no. 12213111 to Y. Nishmura, and no. 14770142 to T. Nakatsura) from the Ministry of Education, Science, Technology, Sports and Culture, Japan.

References

1 Nakatsura T, Senju S, Yamada K, Jotsuka T, Ogawa M, Nishimura Y. Gene cloning of immunogenic antigens overexpressed in pancreatic cancer. *Biochem Biophys Res Commun* 2001; **281**: 936–44.
2 Nakatsura T, Senju S, Ito M, Nishimura Y, Itoh K. Cellular and humoral immune responses to a human pancreatic cancer antigen, coactosin-like protein, originally defined by the SEREX method. *Eur J Immunol* 2002; **32**: 826–36.
3 Monji M, Senju S, Nakatsura T *et al.* Head and neck cancer antigens recognized by the humoral immune system. *Biochem Biophys Res Commun* 2002; **294**: 734–41.
4 Monji M, Nakatsura T, Senju S *et al.* Identification of a novel human cancer/testis antigen, KM-HN-1, recognized by cellular and humoral immune responses. *Clin Cancer Res* 2004; **10**: 6047–57.
5 Kai M, Nakatsura T, Egami H, Senju S, Nishimura Y, Ogawa M. Heat shock protein 105 is overexpressed in a variety of human tumors. *Oncol Rep* 2003; **10**: 1777–82.
6 Srivastava P. Interaction of heat shock proteins with peptides and antigen presenting cells: chaperoning of the innate and adaptive immune responses. *Annu Rev Immunol* 2002; **20**: 395–425.
7 Hickman-Miller HD, Hildebrand WH. The immune response under stress. The role of HSP-derived peptides. *Trends Immunol* 2004; **25**: 427–33.
8 Manjili MH, Henderson R, Wang XY *et al.* Development of a recombinant HSP110-HER-2/neu vaccine using the chaperoning properties of HSP110. *Cancer Res* 2002; **62**: 1737–42.
9 Wang XY, Chen X, Manjili MH, Repasky E, Henderson R, Subjeck JR. Targeted immunotherapy using reconstituted chaperone complexes of heat shock protein 110 and melanoma-associated antigen gp100. *Cancer Res* 2003; **63**: 2553–60.
10 Wang XY, Li Y, Manjili MH, Repasky EA, Pardoll DM, Subjeck JR. Hsp110 over-expression increases the immunogenicity of the murine CT26 colon tumor. *Cancer Immunol Immunother* 2002; **51**: 311–9.
11 Lee-Yoon D, Easton D, Murawski M, Burd R, Subjeck JR. Identification of a major subfamily of large hsp70-like proteins through the cloning of the mammalian 110-kDa heat shock protein. *J Biol Chem* 1995; **270**: 15725–33.
12 Yasuda K, Nakai A, Hatayama T, Nagata K. Cloning and expression of murine high molecular mass heat shock proteins, HSP105. *J Biol Chem* 1995; **270**: 29718–23.
13 Ishihara K, Yasuda K, Hatayama T. Molecular cloning, expression and localization of human 105 kDa heat shock protein, hsp105. *Biochim Biophys Acta* 1999; **1444**: 138–42.
14 Hattori K, Matsushita R, Kimura K, Abe Y, Nakashima E. Synergistic effect of indomethacin with adriamycin and cisplatin on tumor growth. *Biol Pharm Bull* 2001; **24**: 1214–7.
15 Nakatsura T, Kageshita T, Ito S *et al.* Identification of glypican-3 as a novel tumor marker for melanoma. *Clin Cancer Res* 2004; **10**: 6612–21.
16 Yoshitake Y, Nakatsura T, Monji M *et al.* Proliferation potential-related protein, an ideal esophageal cancer antigen for immunotherapy, identified using complementary DNA microarray analysis. *Clin Cancer Res* 2004; **10**: 6437–48.
17 Nakatsura T, Komori H, Kubo T *et al.* Mouse homologue of a novel human oncofetal antigen, glypican-3, evokes T cell-mediated tumor rejection without autoimmune reactions in mice. *Clin Cancer Res* 2004; **10**: 8630–40.
18 Matsuyoshi H, Senju S, Hirata S, Yoshitake Y, Uemura Y, Nishimura Y. Enhanced priming of antigen-specific CTLs in vivo by embryonic stem cell-derived dendritic cells expressing chemokine along with antigenic protein: application to antitumor vaccination. *J Immunol* 2004; **172**: 776–86.
19 Maruyama H, Higuchi N, Nishikawa Y *et al.* High-level expression of naked DNA delivered to rat liver via tail vein injection. *J Gene Med* 2002; **4**: 333–41.
20 Hylander BL, Chen X, Graf PC, Subjeck JR. The distribution and localization of hsp110 in brain. *Brain Res* 2000; **869**: 49–55.
21 Dummer W, Niethammer AG, Baccala R *et al.* T cell homeostatic proliferation elicits effective antitumor autoimmunity. *J Clin Invest* 2002; **110**: 185–92.
22 Maine GN, Mule JJ. Making room for T cells. *J Clin Invest* 2002; **110**: 157–9.
23 Dudley ME, Wunderlich JR, Robbins PF *et al.* Cancer regression and autoimmunity in patients after clonal repopulation with antitumor lymphocytes. *Science* 2002; **298**: 850–4.
24 van der Bruggen P, Traversari C, Chomez P *et al.* A gene encoding an antigen recognized by cytolytic T lymphocytes on a human melanoma. *Science* 1991; **254**: 1643–7.
25 Kawakami Y, Eliyahu S, Delgado CH *et al.* Identification of a human melanoma antigen recognized by tumor-infiltrating lymphocytes associated with in vivo tumor rejection. *Proc Natl Acad Sci USA* 1994; **91**: 6458–62.
26 Chen YT, Gure AO, Tsang S *et al.* Identification of multiple cancer/testis antigens by allogeneic antibody screening of a melanoma cell line library. *Proc Natl Acad Sci USA* 1998; **95**: 6919–23.
27 Rosenberg SA, Yang JC, Schwartzentruber DJ *et al.* Immunologic and therapeutic evaluation of a synthetic peptide vaccine for the treatment of patients with metastatic melanoma. *Nat Med* 1998; **4**: 321–7.
28 Kumar V, Sercarz E. Genetic vaccination: the advantages of going naked. *Nat Med* 1996; **2**: 857–9.
29 Leitner WW, Ying H, Restifo NP. DNA and RNA-based vaccines: principles, progress and prospects. *Vaccine* 1999; **18**: 765–77.
30 Jager E, Chen YT, Drijfhout JW *et al.* Simultaneous humoral and cellular immune response against cancer-testis antigen NY-ESO-1: definition of human histocompatibility leukocyte antigen (HLA)-A2-binding peptide epitopes. *J Exp Med* 1998; **187**: 265–70.
31 Wakatsuki T, Hatayama T. Characteristic expression of 105-kDa heat shock protein (HSP105) in various tissues of nonstressed and heat-stressed rats. *Biol Pharm Bull* 1998; **21**: 905–10.
32 Hatayama T, Yasuda K. Association of HSP105 with HSC70 in high molecular mass complexes in mouse FM3A cells. *Biochem Biophys Res Commun* 1998; **248**: 395–401.
33 Yamagishi N, Nishihori H, Ishihara K, Ohtsuka K, Hatayama T. Modulation of the chaperone activities of Hsc70/Hsp40 by Hsp105alpha and Hsp105beta. *Biochem Biophys Res Commun* 2000; **272**: 850–5.
34 Hatayama T, Yamagishi N, Minobe E, Sakai K. Role of hsp105 in protection against stress-induced apoptosis in neuronal PC12 cells. *Biochem Biophys Res Commun* 2001; **288**: 528–34.
35 Manjili MH, Wang XY, Chen X *et al.* HSP110-HER2/neu chaperone complex vaccine induces protective immunity against spontaneous mammary tumors in HER-2/neu transgenic mice. *J Immunol* 2003; **171**: 4054–61.
36 Gao FG, Khammanivong V, Liu WJ, Leggatt GR, Frazer IH, Fernando GJ. Antigen-specific $CD4^+$ T-cell help is required to activate a memory $CD8^+$ T cell to a fully functional tumor killer cell. *Cancer Res* 2002; **62**: 6438–41.
37 Corthay A, Skovseth DK, Lundin KU *et al.* Primary antitumor immune response mediated by $CD4^+$ T cells. *Immunity* 2005; **22**: 371–83.
38 Zugel U, Schoel B, Yamamoto S, Hengel H, Morein B, Kaufmann SH. Cross recognition by CD8 T cell receptor alpha beta cytotoxic T lymphocytes of peptides in the self and the mycobacterial hsp60 which share intermediate sequence homology. *Eur J Immunol* 1995; **25**: 451–8.
39 Faure O, Graff-Dubois S, Bretaudeau L *et al.* Inducible Hsp70 as target of anticancer immunotherapy: Identification of HLA-A*0201-restricted epitopes. *Int J Cancer* 2004; **108**: 863–70.

ELSEVIER

Journal of the Neurological Sciences 243 (2006) 21 – 30

Journal of the Neurological Sciences

www.elsevier.com/locate/jns

Upregulation of vascular growth factors in multiple sclerosis: Correlation with MRI findings

Jen Jen Su [a], Manabu Osoegawa [a], Takeshi Matsuoka [a], Motozumi Minohara [a], Masahito Tanaka [a], Takaaki Ishizu [a], Futoshi Mihara [b], Takayuki Taniwaki [a], Jun-ichi Kira [a,*]

[a] *Department of Neurology, Neurological Institute, Graduate School of Medical Sciences, Kyushu University, Fukuoka, 812-8582, Japan*
[b] *Department of Radiology, Graduate School of Medical Sciences, Kyushu University, Fukuoka, Japan*

Received 10 June 2005; received in revised form 13 October 2005; accepted 9 November 2005
Available online 27 December 2005

Abstract

Vascular permeability changes precede the development of demyelinating lesions in multiple sclerosis (MS), and vessel wall thickening and capillary proliferation are frequently seen in autopsied MS lesions. Although vascular growth factors are critical for inducing such vascular changes, their involvement in MS has not been extensively studied. Thus, we examined the involvement of various vascular growth factors in MS according to their clinical phase and subtype. We measured serum levels of vascular endothelial growth factor (VEGF), acidic and basic fibroblast growth factors (FGF) and platelet-derived growth factors (PDGFs)-AA, -AB and -BB in 50 patients with MS (27 opticospinal MS and 23 conventional MS patients) and 33 healthy controls using sandwich enzyme immunoassays. Correlations between growth factor changes and brain and spinal cord MRI findings were then analyzed. Serum VEGF concentrations were significantly higher in MS patients in relapse than in controls ($p=0.0495$) and in MS patients in remission ($p=0.0003$), irrespective of clinical subtype. Basic FGF was significantly increased in conventional MS patients, but not opticospinal MS patients compared with controls ($p=0.0291$), irrespective of clinical phase. VEGF at relapse showed a significant positive correlation with the length of spinal cord lesions on MRI ($r=0.506$, $p=0.0319$). The results suggest that an increase in serum VEGF concentration might be involved in MS relapse and the formation of longitudinally extensive spinal cord lesions.

Keywords: OS-MS; C-MS; VEGF; FGF; MRI; Longitudinally extensive spinal cord lesion

1. Introduction

Multiple sclerosis (MS) is an inflammatory demyelinating disease of the central nervous system (CNS). Although the pathological hallmark of this disease is primarily demyelination, a wide variety of pathological changes, such as axonal degeneration, gliosis, remyelination and vascularization, have been noted. In particular, vascular permeability changes are considered crucial since they precede the development of MS lesions [1] and lesions preferentially develop perivascularly [2,3]. However, the precise mechanisms and the molecules responsible for the vascular changes observed in MS are not fully understood [3].

Growth factors are critical for inducing tissue growth and remodeling. Vascular endothelial growth factor (VEGF) induces vascular proliferation as well as vascular permeability changes [4], while platelet-derived growth factor (PDGF) and fibroblast growth factor (FGF) not only induce oligodendroglial progenitor cell growth [5] but also contribute to angiogenesis [6]. Although recent pathological studies have revealed upregulation of VEGF in MS plaques [7], the involvement of growth factors that potentially induce angiogenesis has not been extensively studied in accord with clinical phase and MRI findings.

Two subtypes of MS, distinct in the nature of their CNS pathology, exist in Asians, namely, opticospinal MS (OS-MS) and conventional MS (C-MS). Selective involvement of the optic nerves and spinal cord, and tissue necrosis and conspicuous vascular components are seen in OS-MS, while

* Corresponding author. Tel.: +81 92 642 5340; fax: +81 92 642 5352.
E-mail address: kira@neuro.med.kyushu-u.ac.jp (J. Kira).

0022-510X/$ - see front matter © 2005 Elsevier B.V. All rights reseved.
doi:10.1016/j.jns.2005.11.006

disseminated involvement of the CNS and perivascular demyelination are seen in C-MS [8–10]. These observations prompted us to study serum levels of various growth factors, which might contribute to the vascular changes observed in MS, according to clinical phase and subtype. In addition, we analyzed the correlation between growth factor changes and brain and spinal cord MRI findings, which are distinct between the two subtypes.

2. Subjects and methods

2.1. Subjects

A total of 50 consecutive patients (9 men and 41 women) with relapsing remitting MS, diagnosed according to the criteria of McDonald et al. [11] at the Department of Neurology, Kyushu University Hospital between September 1996 and May 2004, were enrolled in the present study after informed consent was obtained. None were receiving immunomodulatory therapies (interferon beta or immunosuppressants) or high dose corticosteroids (more than 15 mg prednisolone per day) at the time of blood sampling. The mean age at examination was 41.6±16.0 years (mean±S.D.) (range: 17 to 89) and the mean age at disease onset was 33.1±16.2 years (range: 10 to 89). The age at onset and examination had a significant positive correlation ($r=0.751$, $p<0.0001$). All patients were clinically classified as OS-MS or C-MS before sandwich enzyme immunoassays were performed. Briefly, 27 patients whose clinically estimated main lesions were confined to the optic nerves and spinal cord were classified as OS-MS [12]. These patients had no clinical evidence of disease in either the cerebrum or cerebellum, but minor brainstem signs, such as transient double vision and nystagmus, were acceptable.

The remaining 23 patients had multiple involvements of the CNS, including the cerebrum, cerebellum and brainstem, and were classified as C-MS. Disability was evaluated throughout the study by one of the authors (M. Osoegawa) using Kurtzke's Expanded Disability Status Scale (EDSS) score [13], and the progression index (PI) was used for evaluating disease progression; this was calculated by dividing the EDSS score at the last examination by the disease duration [14]. The demographic features of the patients are summarized in Table 1. Sera were obtained at relapse (within 1 month after onset of acute relapse) or remission. Because of limitations of stocked serum volume, from among the 50 MS patients VEGF was measured in 43 samples while other vascular growth factors were also measured in 43. For VEGF assay, 24 serum samples from

Table 1
Clinical and MRI findings of MS patients in this study

	MS ($n=50$)	OS-MS ($n=27$)	C-MS ($n=23$)
Females : males**	41 : 9	27 : 0	14 : 9
Age at disease onset[a,*]	33.1±16.2	37.9±18.1	27.6±11.7
Age at examination[a,*]	41.6±16.0	45.8±16.5	36.7±14.0
Disease duration[a]	8.5±9.3	7.8±8.3	9.1±10.5
EDSS score before peak[b] (stable, relapse)	2.7±2.4	2.8±2.6	2.5±2.2
EDSS score at peak[b] (relapse)	4.6±1.6	4.8±1.7	4.3±1.4
EDSS score at remission[b] (relapse)	3.3±2.2	3.3±2.3	3.3±2.3
Progression index	0.7±1.5	0.8±1.9	0.6±0.8
Brain MRI:			
9 or more T2-high lesions**	28/50 (56.0%)	9/27 (33.3%)	19/23 (82.6%)
Number of T2-high lesions**	9.4±8.6	5.6±5.3	13.7±9.4
1 or more Gd-enhanced lesions	13/50 (26.0%)	5/27 (18.5%)	8/23 (34.8%)
Number of Gd-enhanced lesions	0.3±0.7	0.2±0.4	0.5±0.9
Infratentorial lesion	21/50 (42.0%)	10/27 (37.0%)	11/23 (47.8%)
Juxtacortical lesion	27/50 (54.0%)	12/27 (44.4%)	15/23 (65.2%)
At least 3 periventricular lesions**	25/50 (50.0%)	8/27 (29.6%)	17/23 (73.9%)
Proportion of patients who fulfilled McDonald's MRI criteria*	25/50 (50.0%)	9/27 (33.3%)	16/23 (69.6%)
Number of black holes**	2.0±3.0	0.8±1.0	3.4±3.8
Spinal cord MRI:			
Frequency of spinal cord lesions	32/48 (66.7%)	19/27 (70.4%)	13/21 (61.9%)
Frequency of Gd-enhanced lesions	6/48 (12.5%)	4/27 (14.8%)	2/21 (9.5%)
Spinal cord lesion length[#]	5.0±4.9 cm	6.1±5.7 cm	3.5±3.2 cm
Longitudinally extensive spinal cord lesions	14/48 (29.2%)	11/27 (40.7%)	3/21 (14.3%)

[a]Mean±S.D. (years).
[b]Mean±S.D.
MS=multiple sclerosis; OS-MS=opticospinal MS; C-MS=conventional MS.
EDSS=Expanded Disability Status Scale of Kurtzke; Gd=gadolinium.
*$p<0.05$, **$p<0.01$, for the comparison between OS-MS and C-MS.
[#]Mean±S.D. of the spinal cord lesion length was calculated using only patients with spinal cord lesions on MRI.

23 OS-MS patients, 14 sera at relapse and 10 at remission (1 patient was examined both at relapse and remission), and 19 samples from 19 C-MS patients, 9 at relapse and 10 at remission were tested. For other vascular growth factor assays, 23 serum samples from 23 OS-MS patients, 12 at relapse and 11 at remission and 20 samples from 20 C-MS patients, 9 at relapse and 11 at remission, were examined. A total of 7 MS patients (4 OS-MS and 3 C-MS) were on low dose oral prednisolone at the time of blood sampling (Table 2). Thirty-three healthy subjects (14 men and 19 women) were enrolled as controls. Their average age at sampling was 45.1±17.8 years (range: 21 to 84 years). Age at examination was not different significantly among MS patients in relapse, those in remission and controls, and among OS-MS patients, C-MS patients and controls.

2.2. Sandwich enzyme immunoassays

VEGF, acidic and basic FGFs and PDGFs-AA, -AB and -BB were measured with quantitative sandwich enzyme immunoassays according to the manufacturer's standard protocol (R&D Systems, Minneapolis, MS, USA) by one of the authors (J. J. Su) who was unaware of the diagnoses. Serum samples were thawed from −80 °C to room temperature and assayed in duplicate for the presence of each protein in 96-well polystyrene microtiter plates coated with each capture antibody or a recombinant human PDGF-Rβ/Fc chimera. The assays used each detection antibody conjugated to horseradish peroxidase, and color was developed with tetramethylbenzidine/hydrogen peroxide. The lower detection limits for each protein were as follows: 9 pg/ml for VEGF, 5.68 pg/ml for acidic FGF, 3 pg/ml for basic FGF, 2.07 pg/ml for PDGF-AA, 1.7 pg/ml for PDGF-AB and 15 pg/ml for PDGF-BB.

2.3. Magnetic resonance imaging

All MR studies were performed using 1.5 T units, Magnetom Vision and Symphony (Siemens Medical Systems, Erlangen, Germany) within one month from blood sampling [12]. Typical imaging parameters for brain MRI were: axial T2-weighted turbo spin-echo imaging using TR/TE=2800/90 ms, flip angle=180°; axial turbo-FLAIR imaging using TI/TR/TE=2200/9000/110 ms, flip angle=180°; and sagittal and axial precontrast and axial and coronal postcontrast T1-weighted spin-echo imaging using TR/TE range=400–460/12–17 ms, flip angle range=80–90°. One excitation, a matrix of 256 × 256, a slice thickness of 5 mm, and a slice gap of 2.5 mm were used for all brain studies. Gadopentetate dimeglumine at 0.1 mmol/kg body weight was administered intravenously for contrast-enhanced studies. The typical imaging parameters of the spinal cord were as follows: sagittal T2-weighted turbo spin-echo imaging using TR/TE range=2500–2800/90–116 ms, flip angle=180°, number of excitations=3–4; sagittal T1-weighted spin-echo imaging using TR/TE range=400–440/11–12 ms, flip angle range=90–170°, number of excitations=2–3; axial T2-weighted turbo spin-echo imaging using TR/TE range=3200–5360/99–116 ms, flip angle=180°, number of excitations=3–4; axial T1-weighted spin-echo imaging using TR/TE range=400–440/12 ms, flip angle range=90–170°, number of excitations=2. For sagittal imaging, a matrix of 256 × 256 or 512 × 512, a slice thickness of 4 mm and a slice gap of 0.4 mm were used, and for axial imaging, a matrix of 256 × 256 or 512 × 512, a slice thickness of 5 mm, and a slice gap range of 1.5–5 mm were used. Brain and spinal cord MRI were evaluated independently by two of the authors (F. Mihara and M. Tanaka) who were unaware of the diagnoses. Spinal cord lesions longer than three vertebral lengths were considered longitudinally extensive. Brain MRI lesions were evaluated according to McDonald's MRI criteria for MS [11]. The interval between blood sampling and MRI scanning was less than one month in all cases examined.

2.4. Statistical analysis

The Mann–Whitney *U* test was used for statistical analyses of age at onset, age at blood sampling, disease

Table 2
Clinical data on steroid use of MS patient at the time of blood sampling in this study

	VEGF assay		Other vascular growth factor assay	
At relapse				
No corticosteroid	14 OS-MS		11 OS-MS	
	9 C-MS		9 C-MS	
Low dose corticoid			1 OS-MS	(1:5 mg/day)
At remission				
No corticosteroid	8 OS-MS		8 OS-MS	
	7 C-MS		10 C-MS	
Low dose corticoid	2 OS-MS	(1:5 mg every other day)	3 OS-MS	(1:10 mg/day)
		(1:15 mg/day)		(1:7.5 mg/day)
				(1:5 mg every other day)
	3 C-MS	(1:15/5 mg alternatively)	1 C-MS	(1:5 mg/day)
		(1:5 mg every other day)		
		(1:5 mg/day)		

Number of patients is shown.

duration, EDSS score, PI and length of spinal cord lesions on MRI. Statistical analyses of growth factor levels were initially performed using the Kruskal–Wallis H test for MS patients in relapse, those in remission, and controls, and for OS-MS patients, C-MS patients, and controls. When statistical significance was found, the Mann–Whitney U test was used to determine the statistical differences between each subgroup; uncorrelated p values were corrected by multiplying by the number of comparisons (Bonferroni–Dunn's correction). Spearman's rank correlation test was used to determine correlations between each vascular growth factor, and between clinical parameters and each vascular growth factor. The Chi-square test with Yates' correction or Fisher's exact probability test when the criteria were fulfilled, were used for statistical analyses of the frequency of brain and spinal cord MRI lesions. In all assays, $p<0.05$ was considered statistically significant.

3. Results

3.1. Clinical and neuroimaging findings

The proportion of females with OS-MS was significantly higher than those with C-MS ($p=0.0003$) (Table 1). Ages at disease onset and examination were also significantly higher in OS-MS than C-MS ($p=0.0149$ and $p=0.0438$, respectively). EDSS score at peak and PI were higher in OS-MS than C-MS, although the disease duration was shorter in the former than the latter, but none of these differences reached

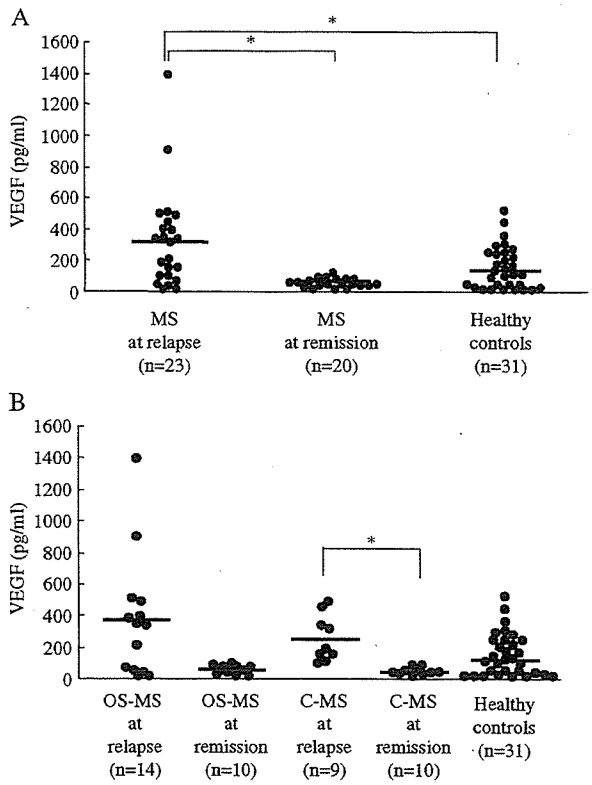

Fig. 2. (A) VEGF concentration in sera of MS patients analyzed separately according to their clinical phase. Bars indicate the mean of each group. *$p<0.05$. (B) VEGF concentration in sera from MS patients analyzed separately according to their clinical subtype and clinical phase. Bars indicate the mean of each group. *$p<0.05$.

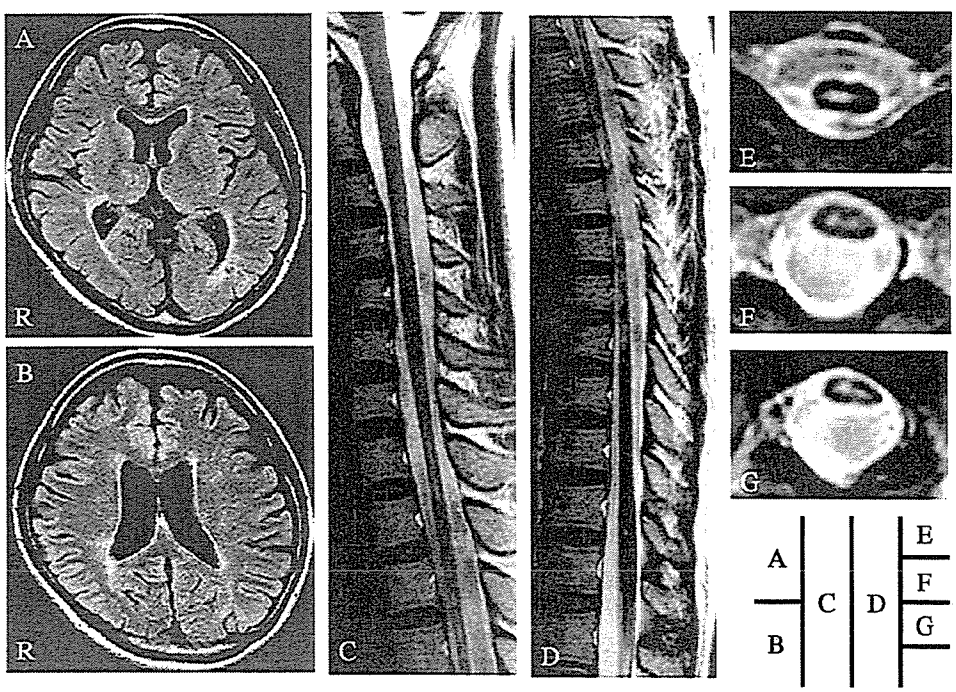

Fig. 1. Representative brain (A, B) and spinal cord MRI (C–G) of a typical OS-MS patient at relapse (disease duration: 4 years). No lesion is visible on T2-weighted axial images of the brain. Longitudinally extensive spinal cord lesion at Th2 to 7 spine levels is shown in T2-weighted sagittal (C, D) and axial (E–G) images of the spinal cord (E: Th1, F: Th3–4 and G: Th4–5 spine levels).

significance. EDSS scores at remission or convalescence did not differ significantly between the two groups.

On brain MRI, the frequency of nine or more T2-hyperintense lesions was significantly higher in C-MS than OS-MS ($p=0.0006$) (Table 1) (Fig.1A and B). Moreover, the frequency of at least three periventricular lesions was also significantly higher in C-MS than OS-MS ($p=0.0015$). However, the frequencies of juxtacortical and infratentorial lesions and gadolinium-enhanced lesions were not significantly different between the two subgroups. Thus, the proportion of patients who fulfilled McDonald's MRI criteria was significantly higher in C-MS than OS-MS ($p=0.0098$). On brain MRI, the frequency of T1 black hole lesions was significantly lower in OS-MS than in C-MS ($p=0.0046$).

On spinal cord MRI, the frequencies of spinal cord lesions were similar between OS-MS and C-MS. The lengths of the spinal cord lesions on MRI were longer in OS-MS than C-MS, though the difference did not reach a statistical significance, and the frequency of longitudinally extensive spinal cord lesions was significantly higher in OS-MS than C-MS ($p=0.0398$) (Table 1) (Fig. 1C–G). Even when seven patients on low dose corticosteroid at the time of blood sampling (4 OS-MS and 3 C-MS) were excluded, essentially the same results were obtained in respect to comparisons between the two subtypes (data not shown).

3.2. Vascular growth factor levels

Serum VEGF concentration was significantly higher in MS patients in relapse (320.5±316.1 pg/ml, mean±S.D.) than in controls (147.3±136.4 pg/ml) ($p=0.0495$) and those in remission (48.6±25.7 pg/ml) ($p=0.0003$) (Fig. 2A). Even when MS patients on the low dose corticosteroids were omitted, the difference between those in relapse and remission was still significant ($p=0.0021$) and the comparison between MS patients in relapse and controls showed a tendency ($p=0.0807$). We then compared serum VEGF levels among OS-MS at relapse, OS-MS at remission, C-MS at relapse, C-MS at remission and healthy controls; a statistically significant difference was found only between C-MS at relapse and at remission, but not in any other comparisons. The difference between OS-MS in relapse and OS-MS in remission lost statistical significance after correction by multiplying the number of comparisons (Fig. 2B). The difference between OS-MS and C-MS patients in relapse also did not reach statistical significance due to the small sample size, although the former was higher (365.0±387.6 vs. 251.2±148.0 pg/ml).

Basic FGF levels did not differ significantly among MS patients in relapse (5.3±4.7 pg/ml), those in remission (5.4±4.2 pg/ml) and controls (3.7±2.5 pg/ml) (Fig. 3A).

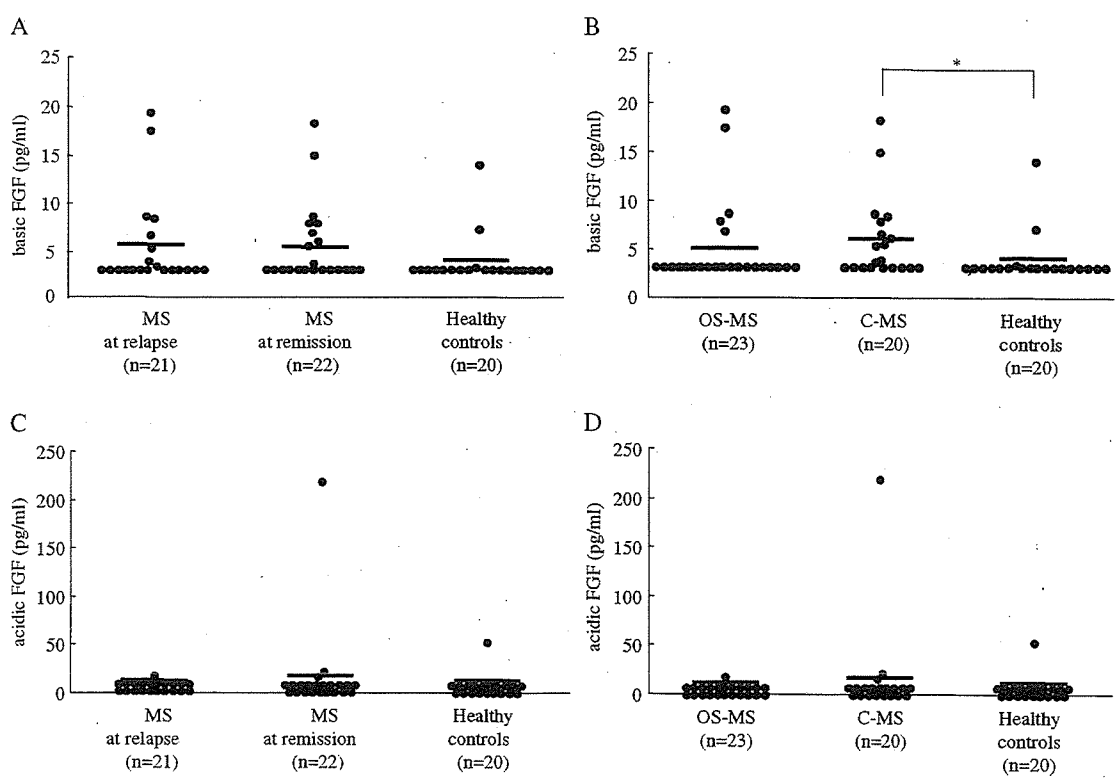

Fig. 3. (A) Basic FGF concentration in sera from MS patients analyzed separately according to their clinical phase. Bars indicate the mean of each group. (B) Basic FGF concentration in sera from MS patients analyzed separately according to their clinical subtype. Bars indicate the mean of each group. *$p<0.05$. (C) Acidic FGF concentration in sera from MS patients analyzed separately according to their clinical phase. Bars indicate the mean of each group. (D) Acidic FGF concentration in sera from MS patients analyzed separately according to their clinical subtypes. Bars indicate the mean of each group.

However, C-MS patients showed a small but significant increase in basic FGF compared with controls (5.8±4.2 vs. 3.7±2.5 pg/ml, $p=0.0291$), irrespective of clinical phase, while no significant change was found in OS-MS patients (5.0±4.5 pg/ml) (Fig. 3B). The difference was still significant even when MS patients on low dose corticosteroids were omitted ($p=0.0189$). No significant changes were detected in any of the other growth factors according to either clinical phase or MS subtype for controls, total MS patients, OS-MS patients, C-MS patients, those in relapse, and those in remission: 8.0±10.4, 24.5±90.7, 6.2±2.3, 45.6±21.2, 6.2±2.5, 41.9±125.7 pg/ml for acidic FGF; 175.2±241.9, 198.4±153.6, 199.8±121.9, 196.7±186.8, 211.9±158.4, 185.5±151.4 pg/ml for PDGF-AA; 375.6±348.6, 386.6±482.3, 420.4± 494.9, 347.6± 477.1, 320.1± 453.8, 450.0±510.4 pg/ml for PDGF-AB; and 215.0±289.9, 196.0±191.9, 162.2±162.5, 234.8±218.7, 157.1± 214.2, 233.1±164.3 pg/ml for PDGF-BB, respectively (Fig. 3C, B and Fig. 4). There was a significant positive correlation between acidic and basic FGF ($p=0.0199$) and between PDGF-AB and -BB ($p<0.0001$), but not -AA, while there were no correlations between VEGF and any other vascular growth factor.

3.3. Correlation among vascular growth factor levels, clinical features and neuroimaging findings

As shown in Fig. 5, when vascular growth factor levels were plotted against the time interval between the onset day of relapse and blood sampling, only VEGF showed a sharp rise at the time of relapse (within one month after the onset). One OS-MS patient whose VEGF levels were

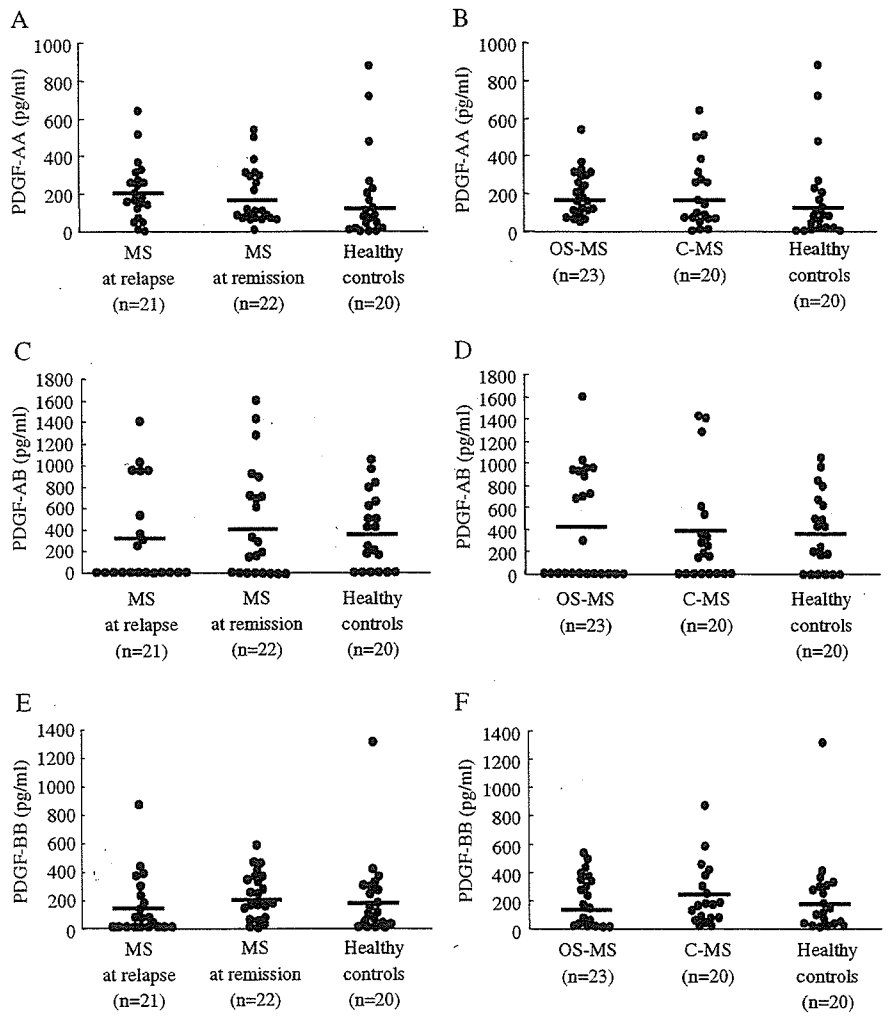

Fig. 4. (A) PDGF-AA concentration in sera of MS patients analyzed separately according to their clinical phase. Bars indicate the mean of each group. (B) PDGF-AA concentration in sera of MS patients analyzed separately according to their clinical subtype. Bars indicate the mean of each group. (C) PDGF-AB concentration in sera of MS patients analyzed separately according to their clinical phase. Bars indicate the mean of each group. (D) PDGF-AB concentration in sera of MS patients analyzed separately according to their clinical subtype. Bars indicate the mean of each group. (E) PDGF-BB concentration in sera of MS patients analyzed separately according to their clinical phase. Bars indicate the mean of each group. (F) PDGF-BB concentration in sera of MS patients analyzed separately according to their clinical subtype. Bars indicate the mean of each group.